Energy & Environmental Science

RSC Publishing

REVIEW

Update on Na-based battery materials. A growing research path

Cite this: *Energy Environ. Sci.*, 2013, **6**, 2312

Verónica Palomares,[a] Montse Casas-Cabanas,[b] Elizabeth Castillo-Martínez,[b] Man H. Han[b] and Teófilo Rojo*[ab]

Received 26th March 2013
Accepted 14th June 2013

DOI: 10.1039/c3ee41031e

www.rsc.org/ees

This work presents an up-to-date information on Na-based battery materials. On the one hand, it explores the feasibility of two novel energy storage systems: Na-aqueous batteries and Na–O_2 technology. On the other hand, it summarises new advances on non-aqueous Na-ion systems. Although all of them can be placed under the umbrella of Na-based systems, aqueous and oxygen-based batteries are arising technologies with increasing significance in energy storage research, while non-aqueous sodium-ion technology has become one of the most important research lines in this field. These systems meet different requirements of energy storage: Na-aqueous batteries will have a determining role as a low cost and safer technology; Na–O_2 systems can be the key technology to overcome the need for high energy density storage devices; and non-aqueous Na-ion batteries have application in the field of stationary energy storage.

Broader context

Current interest in Na-ion based batteries arises from the potential of these devices to become less expensive, safer and environmentally benign with respect to present Li-ion technologies. Proof of this potential is the number of publications that have been devoted to Na-ion battery materials during the last and present year. This article provides an update on our previous review (T. Rojo *et al.*, *Energy Environ. Sci.*, 2012, **5**, 5884–5901) that aims to cover the most significant advances on electrode materials as well as on other new related systems such as aqueous and Na–O_2 batteries.

1 Introduction

In a world with a growing concern about energy management issues, sodium has strongly broken into energy storage research field. This alkali holds promise for being a complement or substituting Li-based technology. Its natural abundance, easy access to sodium sources and, consequently, lower price; suitable redox potential ($E^0_{(Na+/Na)} = -2.71$ V *vs.* standard hydrogen electrode, 0.3 V above that of Li) and similar intercalation chemistry to Li, make this element strategic in innovative research of energy storage systems.

Sodium has already been successfully used in high temperature storage technologies, such as sodium–sulfur and ZEBRA batteries. Sodium–sulfur batteries, developed since 1980s, utilize molten sodium and sulfur as anode and cathode which are separated with a β-alumina solid electrolyte and usually operate at 300–350 °C. The advantages of this kind of battery are high power and energy densities, temperature stability, low cost and easiness to recycle its components. Its main disadvantages are the risk of an uncontained reaction in case of electrolyte breaking, and the corrosion produced by the molten electrodes, that involves the use of highly resistant containers such as chromized steel and molybdenum-lined steels.[1] These features make this system useful only for stationary energy storage. On the contrary, ZEBRA batteries, that operate at about 300 °C, can be employed both in static storage and in electric vehicles due to their enhanced safety. These cells are made of a molten sodium anode, a metal chloride positive electrode ($NiCl_2$, $FeCl_2$) and β″-Al_2O_3 as electrolyte and separator. This way, there is no risk of unexpected reaction if the ceramic electrolyte breaks. This system presents high operating voltages, good tolerance against overcharging and easiness of assembly in the discharged state. Up to date research on this kind of sodium batteries involves lowering operating temperature at least below 170 °C. Getting this aim comprises the design of new electrolytes that present good Na^+ conducting properties at lower temperatures. This latter point is extensively described in a recent review by K. B. Hueso *et al.*[2]

In the last two years, new research lines in room temperature energy storage based on sodium have arisen, namely Na-ion and Na–O_2 batteries. One year ago we published a review article gathering all the information about electrodes and electrolytes for this kind of batteries.[3] The present work intends to be an update on that text, describing the main advances made on this

[a]*Departamento de Química Inorgánica, Universidad del País Vasco UPV/EHU, P.O. Box. 644, 48080, Bilbao, Spain. Fax: +34 946013500; Tel: +34 946012458*

[b]*CIC ENERGIGUNE, Parque Tecnológico de Álava, Albert Einstein 48, ED.CIC, 01510, Miñano, Spain. E-mail: trojo@cicenergigune.com; Tel: +34 945297108*

field during the last year, the new systems that have appeared, and analyzing the possible future trends that can be key points to move closer to a commercial Na-ion battery.

Verónica Palomares (1981, Bilbao) received her Ph.D. in Chemistry from the University of the Basque Country (UPV/EHU) in 2009. During her Ph.D. she worked on nanostructured cathodes for Li-ion batteries in collaboration with Cidetec-IK4. Recently, she has been Associate Professor at the UPV/EHU. At the moment she is a Post-doctoral Researcher at the University of the Basque Country, and works in the field of new electrode materials for sodium ion batteries.

Montse Casas-Cabanas completed her Ph.D. in Materials Science at the Institut de Ciència de Materiales de Barcelona (Spain) in 2006. Afterwards, she joined LRCS (Amiens, France) as a post-doctoral researcher working in the crystallochemical characterization of lithium-ion battery materials from powder diffraction and spent one year at Electron Microscopy for Materials Science Institute (Antwerp, Belgium). Before joining CIC energiGUNE she was Maître des Conferences at Laboratoire de Cristallographie et Sciences des Materiaux (Caen, France) working on energy related materials. Her research focuses on the study of new materials for energy storage and the impact of structure and microstructure in their electrochemical properties.

Elizabeth Castillo Martinez received her Ph.D. in Chemistry from University Complutense, Madrid, in 2008, under the supervision of Professor Miguel Angel Alario on high pressure synthesis and characterization of metal oxides. She then spent two years at the NanoTech Institute of the University of Texas with Professor Ray H. Baughman, working in diverse areas related to energy. In 2011 she worked as a visiting scientist at the University of Cambridge with Professor Clare Grey, on the investigation of electrode materials for Li-ion batteries by solid state NMR, and is currently working at CIC energiGUNE as a PostDoctoral researcher.

Organic liquid electrolytes will be commented on within the anodes version, while polymer electrolytes will not be shown in a distinct section, because new advances on this topic are scarce, and only a patent by Villaluenga *et al.*[4] and two articles must be mentioned.[5]

2 Na-ion aqueous batteries

The most promising approach to reduce costs in Na-based systems is the use of a Na-ion electrode in an aqueous electrolyte. Aqueous electrolytes have much higher ionic mobility than organic solvents, are cheaper, the devices are simpler to manufacture and can be produced with thicker electrodes. Although the lower potential range of water puts a limit upon the possible cell voltage, the potential advantages in terms of cost are extremely appealing. In addition, these systems would be safer than the current organic solvent based batteries.

The electrochemical behaviour of a Na insertion electrode material in an aqueous electrolyte has been reported for very

Man H. Han received his undergraduate degree in Chemistry from the Georgia Institute of Technology in Atlanta. He completed his Ph.D. in Inorganic Materials Chemistry at the Georgia Institute of Technology in 2008, where his thesis focused on synthesis and characterization of magnetic nanoparticles. He has extensive research experience with synthesis of various inorganic nanomaterials, Li-ion battery materials, surface modification, nanocomposites and their applications. Upon his graduation, he was employed at KaMin LLC as analytical chemist and is currently working at CIC energiGUNE as a PostDoctoral researcher.

Teófilo Rojo received his Ph.D. from the University of the Basque Country in 1981. He has spent various research periods at several European and American universities. Since 1992 he has been Full Professor of Inorganic Chemistry at the UPV-EHU. His research has been focused on solid state chemistry and materials science. Since 2010 he has been the Scientific Director of the CIC EnergiGUNE and his research is focused on the study of materials for both lithium and non-lithium based batteries. He holds different positions in various scientific bodies in Spain being the chairman of the Solid State Chemistry Group within the Spanish Royal Society during the last ten years.

few materials. One of the first reports is that of Sauvage *et al.*, who tested the electrochemical insertion/de-insertion of Na into $Na_{0.44}MnO_2$ in aqueous media when studying this material for its sensing properties.[6] They observed three different phenomena between −0.05 and 0.85 V *vs.* SCE (standard calomel electrode) linked to phase transitions between structurally close phases, and were able to cycle this material between $0.25 < x < 0.44$. They also reported a compositional change when ageing $Na_{0.44}MnO_2$ in the electrolyte solution ($NaNO_3$ 0.01 M) as the Na/Mn ratio drops to 0.33 without this affecting the electrochemical properties.

An interesting approach is that of Whitacre *et al.* who used $Na_{0.44}MnO_2$ as a positive electrode in a hybrid energy storage device.[7] In this cell, activated carbon was chosen as anode material, storing charge though a nonfaradaic or capacitive reaction of anions on its surface, and Na_2SO_4 1 M as electrolyte. These hybrid devices offer higher energy densities than supercapacitors while keeping the reversibility of the system extremely high. In this case, the system was cycled through a potential range of approximately 0.5 V from $Na_{0.44}MnO_2$ to $Na_{0.22}MnO_2$, showing a specific capacity of 45 mA h g^{-1}. The resulting full cell is cycled within a potential window of 1.4 V and a very good cyclability for 1000 cycles was demonstrated.[8–10]

Improved results on this type of cells have been reported when using λ-MnO_2,[11] as this material is able to deliver a specific capacity up to 100 mA h g^{-1}. Despite this material being prepared by acidic treatment of a lithium containing material, $LiMn_2O_4$, the authors calculate that its higher energy density results in a much lower specific cost in \$ A h^{-1} than $Na_{0.44}MnO_2$. A cell tested using thick electrodes delivered 25 W h kg^{-1} in less than 5 h of discharge. Aquion Energy is commercially developing this concept and the first devices will be available this year.[12]

Wessells *et al.* have proposed copper and nickel hexacyanoferrates ($KCuFe(CN)_6$ and $KNiFe(CN)_6$) as positive electrode materials for K^+ and Na^+ aqueous batteries.[13,14] These materials are Prussian Blue analogues and crystallize in an open framework of general formula $A_xPR(CN)_6$ ($0 \leq x \leq 2$) in which P^{+m} and R^{+n} coordinate to the nitrogen and carbon ends of the CN-group respectively, while A atoms can be intercalated in the interstitial sites that result from the large cages (see Fig. 1). These materials have a theoretical specific capacity of about 60 mA h g^{-1} (although it might vary due to variations in zeolitic water content). $KNiFe(CN)_6$ was found to react with sodium at 0.59 V *vs.* SHE (standard hydrogen electrode) while $KCuFe(CN)_6$ reacts at 0.77 V, in addition to a second process that is observed near 1.0 V. Promising rate capabilities, round trip energy efficiencies and cyclabilities are shown.[14] A start-up company, Alveo Energy, is looking to develop low cost batteries based on these materials.

A more fundamental work has studied the co-insertion of different ions from mixed electrolyte solutions and their coexistence in the electrode matrix. To do so, electrochemical Quartz Crystal has been applied to the model system (Li,Na)$FePO_4$/$FePO_4$ in mixed aqueous electrolyte solutions of lithium and sodium sulfates and a high selectivity of Li-ions insertion into $FePO_4$ as compared to that of Na-ions has been found.[15]

Negative electrode materials are less explored although promising results have been obtained using $NaTi_2(PO_4)_3$. This material operates within the stability window of the electrolyte (approximately 0.5 V before H_2 evolution in NaOH 4 M) and, similar to the results obtained in organic electrolyte, is able to deliver around 120 mA h g^{-1}.[16] A full Na-ion battery has been tested using $Na_{0.44}MnO_2$ in the positive side.[17] The cells can be cycled between 0.5 and 1.4 V at very high rates (over 100 C) and exhibit excellent cyclability when cycled at high rates, although capacity fades when cycled below 1 C.

3 Na-ion non-aqueous battery materials

3.1 Cathodes

A great range of compounds are being studied as possible cathodic materials for Na-ion batteries, from oxides to phosphates, fluorophosphates or pyrophosphates. Each family of compounds presents its own advantages and disadvantages for their real application in energy storage systems. The following sections explain the main features of each one.

3.1.1 $NaMO_2$ oxides

Layered structure oxides. The layered $NaMO_2$ (M = Ni, Mn, Cr, Co, V, *etc.*) compounds are considered to be a promising cathode system for Na-ion batteries due to their high capacity, material cost, and safety. Their crystal structure is similar to that of layered $LiMO_2$ where Li ions lie between the sheets of edge-shared MO_6 octahedra. Due to their crystallographic nature, layered $NaMO_2$ compounds are very sensitive in ambient conditions and absorb water molecules into the interslab space. Regardless, the chemistry of Na layered materials is expected to be different from their Li analogue due to its larger ionic radius (Li^+: 0.76 Å, Na^+: 1.02 Å). Unlike the Li analogue, $NaMO_2$ forms well-structured layered compounds and is expected not to suffer from severe irreversible capacity loss caused by structural changes upon extensive electrochemical cycling. Like their lithium counterparts, the layered oxides are classified based on the sequence of oxygen stacking and each type exhibits slightly different electrochemical performances. For example, in a P2-phase Na occupies the trigonal prismatic sites (P, entirely face sharing or entirely edge sharing) of ABBA oxygen stacking sequence (Fig. 2a). Another example is O3-phase, where Na occupies octahedral sites (O, face sharing) with ABC oxygen stacking (Fig. 2b). Typically, P2 is accepted as a better cathode because of their high diffusion rate and prohibited slab-gliding.

There is a wide range of transition metals and their combinations that can lead to layered $NaMO_2$ compounds, as can be seen in Fig. 3. Each of them possesses a different operating voltage and specific capacity, which defines its energy density.[18]

In the first place, monoclinic O3-type $NaNiO_2$ has been reinvestigated by several researchers. Fielden and Obrovac reported an irreversible capacity of 40 mA h g^{-1} and a reversible capacity of 80 mA h g^{-1} within the voltage range of 2.0–3.5 V at C/10 after the first cycle.[19] Vassilaras *et al.* investigated the same system and showed that a larger amount of Na can be deintercalated/intercalated.[20] Multiple *plateaux* were observed due

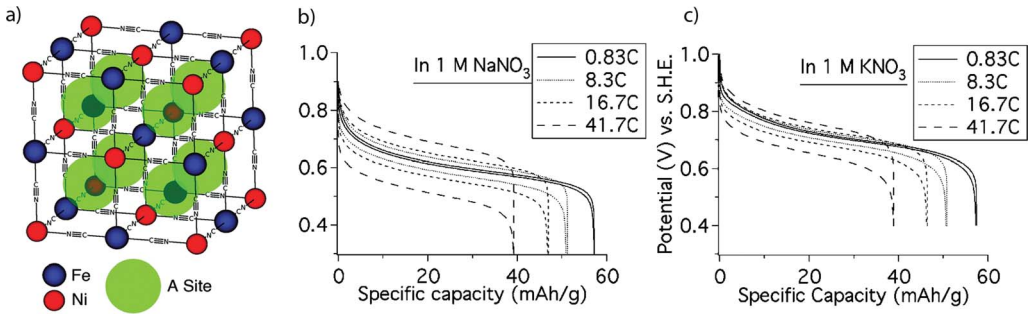

Fig. 1 (a) Prussian Blue crystal structure; (b) and (c) potential profiles of NiHCF during galvanostatic cycling of Na^+ and K^+ at various rates (reprinted with permission from C. D. Wessells, S. V. Peddada, R. A. Huggins, and Y. Cui, *Nano Lett.*, 2011, **11**, 5421–5425. Copyright 2011 American Chemical Society).

to phase change during charge/discharge cycles (Fig. 4). Overall, a 147 mA h g^{-1} discharge capacity (0.62Na) within the voltage range of 2.0–4.5 V at C/10 were achieved. However, large capacity loss was observed probably due to an irreversible phase change which is evidenced by the formation of an unidentifiable phase after cycling. Cycling the cell over the voltage range of 1.25–3.75 V resulted in a 123 mA h g^{-1} discharge capacity (0.52 Na) with fairly stable capacity retention at C/10. Significant improvement in coulombic efficiency at lower cut-off voltage indicated that the phase changes below 3.75 V are highly reversible although the fully sodiated phase is never achieved and $Na_{0.91}NiO_2$ is obtained instead.

Besides, O3-type α-$NaFeO_2$, one of the classic examples of layered $NaMO_2$, has also been revisited as positive electrode.[21] Cut-off voltage during the charging significantly influences the reversibility of α-$NaFeO_2$. Similar to $NaNiO_2$, the charge capacity increases at high cut-off voltages but the reversible capacity significantly decreases when charged above 3.5 V. At or below a charge voltage of 3.4 V, the cell exhibited good capacity retention with reversible specific capacity up to 80 mA h g^{-1} (0.3Na). XRD study of cycled cathodes revealed significant irreversible structural changes, which were caused by migration of iron into the interslab space at high voltage.

On the other hand, Chen *et al.* reported electrochemistry of $NaCrO_2$,[22] a layered rock salt structure identical to α-$NaFeO_2$. The specific capacity reached 100 mA h g^{-1} at 15 mA g^{-1} current and 119 mA h g^{-1} at 2 mA h g^{-1} (approximately 0.4 Na were exchanged). Multiple *plateaux* were observed due to structural changes. In order to study the effect of surface coating, carbon coated $NaCrO_2$ was synthesized by Ding *et al.*[23] using citric acid in a solid-state reaction. Carbon coated $NaCrO_2$ maintained a stable 100 mA h g^{-1} discharge specific capacity after 40 cycles as opposed to rapid capacity fading of nearly 20% after 20 cycles in previous reports.[24] The multiple peaks on the CV curve (Fig. 5) were identified to be a phase change from hexagonal O3 to monoclinic O3 to monoclinic P3 and the sharp peaks were associated with partial oxidation of Cr^{3+} to Cr^{4+}. The better performance of coated particles is due to the fact that the cover prevents direct contact between the active material and the electrolyte. This coating effectively reduces side reactions between the electrode material and the electrolyte and decreases the polarization by increasing electronic conductivity.[25,26]

P2-Na_xCoO_2 has been speculated as an excellent cathode material due to superb electrochemical performance of its Li

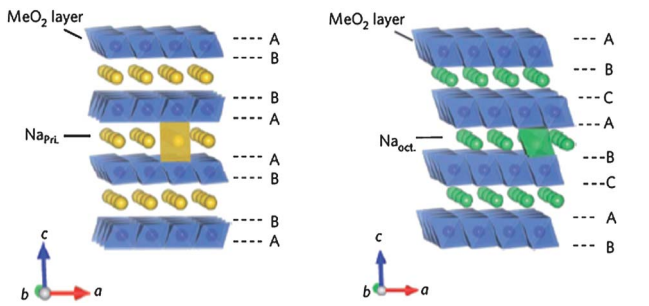

Fig. 2 Layered structure of P2-type (left) and O3-type (right) $NaMO_2$. Reprinted by permission from Macmillan Publishers Ltd: N. Yabuuchi, M. Kajiyama, J. Iwatate, H. Nishikawa, S. Hitomi, R. Okuyama, R. Usui, Y. Yamada and S. Komaba, *Nat. Mater.*, **11**, 512–517. Copyright 2012.

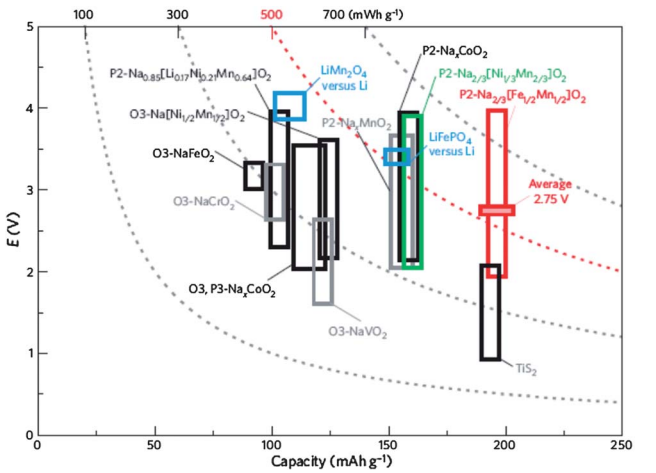

Fig. 3 A comparison of reversible capacity and operating voltage ranges of the layered sodium insertion materials. The energy density was calculated on the basis of the voltage *versus* metallic sodium for simplicity. $LiFePO_4$ and $LiMn_2O_4$ are also shown for comparison based on the voltage *versus* Li metal. Reprinted by permission from Macmillan Publishers Ltd: N. Yabuuchi, M. Kajiyama, J. Iwatate, H. Nishikawa, S. Hitomi, R. Okuyama, R. Usui, Y. Yamada and S. Komaba, *Nat. Mater.*, **11**, 512–517. Copyright 2012.

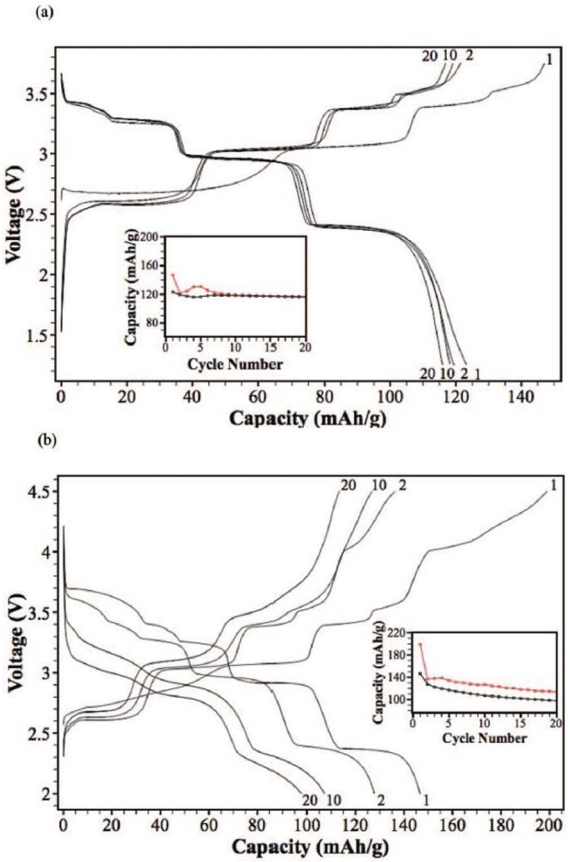

Fig. 4 Voltage profile of $NaNiO_2$ after multiple cycles at C/10. The cell is galvanostatically cycled between (a) 1.25–3.75 V, and (b) 2.0–4.5 V. Reproduced by permission of The Electrochemical Society from P. Vassilaras, X. Ma, X. Lin and G. Ceder, *J. Electrochem. Soc.*, 2013, **160**, A207–A211.

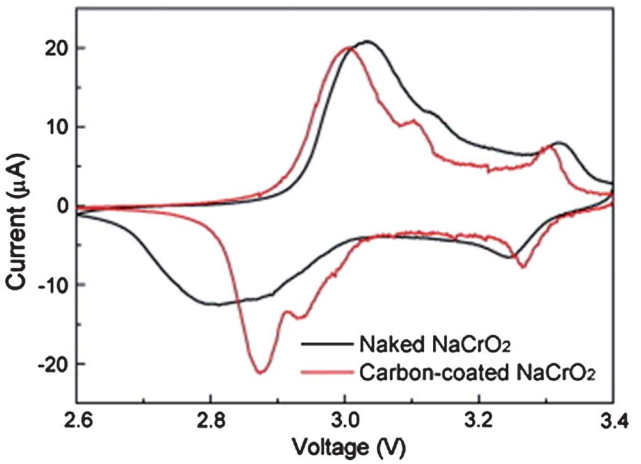

Fig. 5 Cyclic voltammogram for $NaCrO_2/NaClO_4/Na$ cell between 2.6 and 3.4 V at a scan rate of 0.1 mV s^{-1}. Reprinted from J. J. Ding, Y. N. Zhou, Q. Sun and Z. W. Fu, Cycle performance improvement of $NaCrO_2$ cathode by carbon coating for sodium ion batteries, *Electrochem. Commun.*, **22**, 85–88. Copyright 2012, with permission from Elsevier.

analogue, although the high cost of cobalt makes its commercialization nonviable. In an effort to understand the effect of ionic diffusion length and particle size, the electrochemical properties of two P2-$Na_{0.71}CoO_2$ samples with different microstructure were reported.[27] The cathode with smaller dimensions exhibited a specific capacity of 105 mA h g^{-1} within the voltage range of 2.0–3.9 V at C/25, while the cathode with larger dimensions achieved 70 mA h g^{-1} with the same voltage ranges and the same C-rates. In addition, higher capacity retention and less polarization were also obtained with the smaller particles. These results are indicative of better kinetics due to smaller particle dimensions which induces a shorter ionic diffusion path.

Ding *et al.* studied a similar composition of P2-type $Na_{0.74}CoO_2$ as cathode material,[28] achieving a discharge capacity of 107 mA h g^{-1} ($Na_{0.93}CoO_2$) at C/10 within the cycling voltage of 2.0–3.8 V (Fig. 6a). A capacity of 55.7 mA h g^{-1} ($Na_{0.5}CoO_2$) could also be obtained when starting on charge. Multiple *plateaux* at 2.72 V, 3.00 V, 3.30 V, and 3.60 V were observed, which implied a series of phase changes while cycling. The voltage polarization of 150–250 mV was much higher than that of Li_xCoO_2 counterpart. Interestingly, coulombic efficiency of the cell with $NaClO_4$ electrolyte was higher than that of $NaPF_6$. Regardless of the electrolyte, the coulombic efficiency was reported to be very consistent up to 40 cycles (Fig. 6b). *Ex situ* XRD study showed expansion and compression in the *c*-axis upon cycling, which proves stable deintercalation and intercalation of Na^+ in the inter-slab space. XPS (X-ray photoelectron spectroscopy) measurement confirmed Co^{3+}/Co^{4+} redox reaction.

In an effort to improve the electrochemical performance of layered oxide materials, transition metal mixtures have also been studied extensively. Lee *et al.* investigated the electrochemistry of P2-type $Na_{2/3}[Ni_{1/3}Mn_{2/3}]O_2$.[29] This oxide exhibited charge/discharge capacity of 150 mA h g^{-1} (2/3 Na can be cycled), but poor cycling and rate capability was observed above 4.2 V due to irreversible phase change. Below 4.2 V, excellent cycling property at C/20 and C/2 was observed for 20 cycles.

Komaba *et al.* reported the electrochemical behaviour of $NaNi_{0.5}Mn_{0.5}O_2$ system.[30] The cell could deliver more than 185 mA h g^{-1} capacity when fully desodiated between 2 and 4.5 V, but reversibility was insufficient due to significant expansion of the interslab space. When cycled in the voltage range of 2.2–3.8 V, the cathode exhibited 105 mA h g^{-1} at 1 C and 125 mA h g^{-1} at C/50 and showed 75% of the initial capacity retention after 50 cycles. An *ex situ* XRD study showed that the original O3 phase and O′3 (monoclinic distorted) coexist up to $x = 0.2$ Na extraction while the O′3 phase disappears at $x = 0.3$ and P3 dominates. At $0.45 < x$ 0.55, P′3 exists and at $x >$ 0.55 P′3 and P3″ coexist. In this case, it was demonstrated by XAS analysis (X-ray absorption spectroscopy) that the electrochemical behaviour was solely dependent of the redox reaction of divalent Ni and that tetravalent Mn was electrochemically inactive.

Thorne *et al.* reported $Na_{0.75}Fe_{0.75}Mn_{0.25}O_2$ (ref. 31) phase with a charge capacity of 131 mA h g^{-1}. Yabuuchi *et al.* compared the electrochemical behaviour of P2 and O3-type

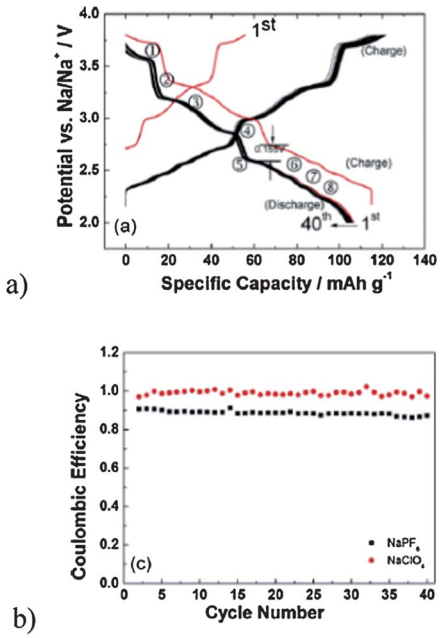

Fig. 6 (a) Galvanostatic curves of P2-$Na_{0.74}CoO_2$/$NaPF_6$/Na cells at a current rate of C/10 and (b) coulombic efficiency of the cells as a function of the cycle number. Reprinted from J. J. Ding, Y. N. Zhou, Q. Sun, X. Q. Yu, X. Q. Yang and Z. W. Fu, Electrochemical properties of P2-phase $Na_{0.74}CoO_2$ compounds as cathode material for rechargeable sodium-ion batteries, *Electrochim. Acta*, 2013, **87**, 388–393, Copyright 2013, with permission from Elsevier.

$Na_x[Fe_{1/2}Mn_{1/2}]O_2$ ($x = 2/3$ and 1, respectively).[18] P2- and O3-type were prepared as single phase. O3-type $Na[Fe_{1/2}Mn_{1/2}]O_2$ delivered 100–110 mA h g^{-1} in the voltage range of 1.5–4.2 V at C/20 with large polarization at approximately 1 V, while P2-type $Na_{2/3}[Fe_{1/2}Mn_{1/2}]O_2$ displayed a high capacity value of 190 mA h g^{-1} with the same condition, which is 72% of the theoretical capacity based on [M^{3+}/M^{4+}] process (Fig. 7a). The capacity retention *vs.* cycle number of both electrodes showed similar behaviour (Fig. 7b) with relatively good capacity retention, which implies that the structural transformations do not degrade the material upon cycling.

Kim *et al.* reported the electrochemical properties of $Na(Ni_{1/3}Fe_{1/3}Mn_{1/3})O_2$, isostructural to α-$NaFeO_2$.[32] The full cell $Na_yC/Na_{1-y}(Ni_{1/3}Fe_{1/3}Mn_{1/3})O_2$ showed an average OCV (open circuit voltage) of 2.75 V with a capacity maintained at about 100 mA h g^{-1} for 150 cycles at 1.–5–4.0 V at C/2 (Fig. 8). XRD pattern of a cycled cathode (123 cycles) revealed that the $R\bar{3}m$ layered structure was stable after extensive cycling.

Sathiya *et al.* reported the electrochemical behaviour of O3-type $NaNi_{1/3}Mn_{1/3}Co_{1/3}O_2$.[33] The cell reached reversible intercalation of 120 mA h g^{-1} (0.5 Na^+) in the voltage range of 2–3.75 V at C/10. Also, the capacity loss was minimal even after 50 cycles. The evolution of this material during electrochemical reaction was followed by *in situ* XRD, showing a O3–O1–P3–P1 transition (Fig. 9). To be more precise, O3–O1 transition occurred at $1 < x < 0.9$. Biphasic domain (O1 + P3) appeared at $0.9 < x < 0.82$, and a small biphasic region (P1 + P3) appeared between $0.67 < x < 0.6$. P3 phase solely existed when $x < 0.60$. The stability of the compound under atmospheric conditions was studied by XRD and a phase transition from O3 to O1 (15 days) to P3 (30 days) was observed. This transition was due to the extensive amount of atmospheric water molecule absorbed, which effectively increased the inter-slab distance and induced the phase change.

Didier *et al.* reported the electrochemistry of O′3-type $NaVO_2$.[34] The deintercalation/intercalation reaction was reversible in the $\frac{1}{2} \leq x \leq 1$ range, and in the range $\frac{1}{2} \leq x \leq 2/3$ (C/100), complex biphasic domain occurred. A detailed XRD study revealed that as Na^+ was extracted from the crystal, the inter-slab distance increased gradually due to the increasing oxygen repulsion.

One of the most significant efforts to improve the electrochemical performance of layered oxides is to stabilize the inter-slab space by metal substitution. Yuan *et al.* compared the electrochemical performance of P2-phase $Na_{0.67}[Mn_{0.65}Ni_{0.15}Co_{0.2}]O_2$ (NaMNC) and Al-substituted $Na_{0.67}[Mn_{0.65}Ni_{0.15}Co_{0.15}Al_{0.05}]O_2$(NaMNCA) using a citric acid assisted combustion method.[35] The resultant particles formed microflakes with almost the same XRD features and peaks compared to unsubstituted P2-$Na_{2/3}MnO_2$ and $Na_{2/3}[Mn_{1-x}Ni_x]O_2$.[36] The CV (cyclic voltammetry) curve of NaMNC indicated that there are three pairs of reversible redox peaks at the potentials of 4.25, 3.65 and 2.3 V, corresponding to the redox reaction of Ni^{2+}/Ni^{4+}, Co^{3+}/Co^{4+}, and Mn^{3+}/Mn^{4+}, respectively. NAMNC provided 141 mA h g^{-1} at 20 mA g^{-1} between 2 and 4 V, losing 11% of the specific capacity in the first 30 cycles. The capacity retention became stable after the 30th cycle.

On the other hand, NaMNCA exhibited almost identical CV features as NaMNC except for the small splitting of the

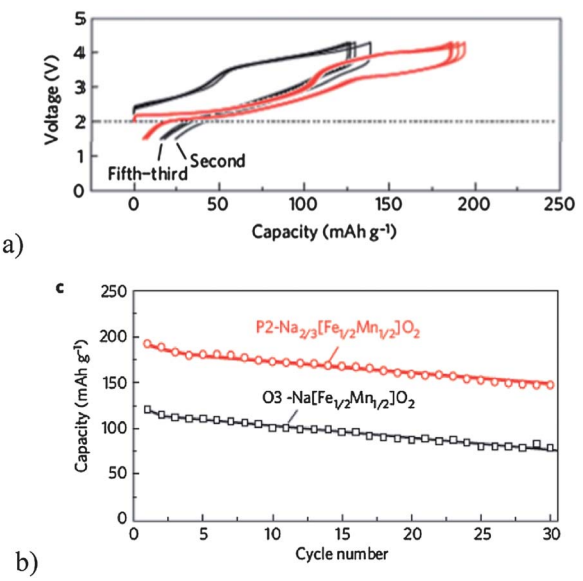

Fig. 7 (a) Galvanostatic charge/discharge (oxidation/reduction) curves for Na/$Na[Fe_{1/2}Mn_{1/2}]O_2$ and Na/$Na_{2/3}[Fe_{1/2}Mn_{1/2}]O_2$ cells at a rate of 12 mA g^{-1} in the voltage range of 1.5 and 4.3 V; and (b) comparison of the discharge capacity retention of the sodium cells. Reprinted by permission from Macmillan Publishers Ltd: N. Yabuuchi, M. Kajiyama, J. Iwatate, H. Nishikawa, S. Hitomi, R. Okuyama, R. Usui, Y. Yamada and S. Komaba, *Nat. Mater.*, 2012, **11**, 512–517. Copyright 2012.

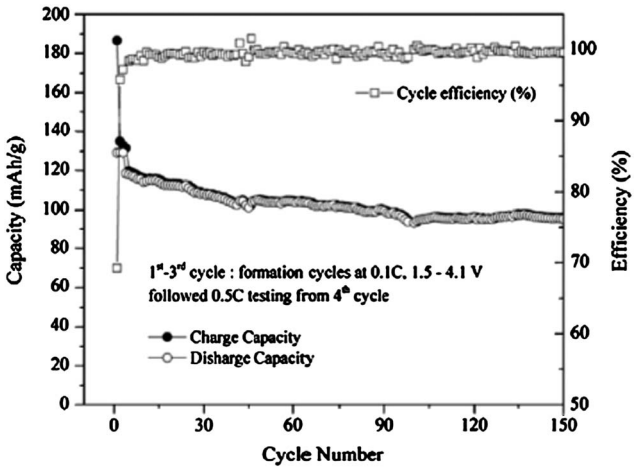

Fig. 8 Long term cycling and coulombic efficiency of Na-ion $Na_yC/Na_{1-y}(Ni_{1/3}Fe_{1/3}Mn_{1/3})O_2$ cell. Following the 4th cycle, the full cell was continuously cycled at a charge–discharge 0.5 C rate (75 mA g^{-1}) between 1.5 and 4.1 V. Reprinted from D. Kim, E. Lee, M. Slater, W. Lu, S. Rood and C. S. Johnson, Layered $Na[Ni_{1/3}Fe_{1/3}Mn_{1/3}]O_2$ cathodes for Na-ion battery application, *Electrochem Commun.*, 2012, **18**, 66–69, Copyright 2012, with permission from Elsevier.

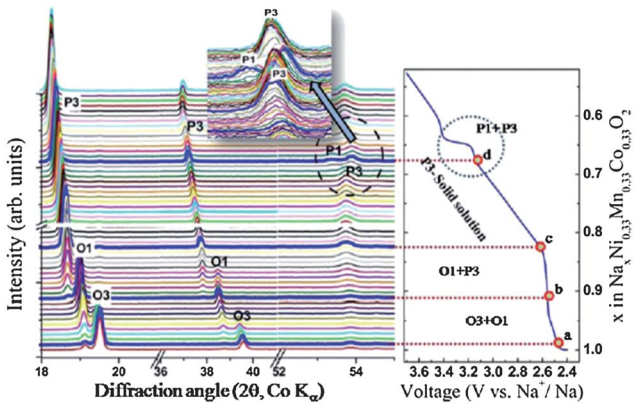

Fig. 9 *In situ* X-ray diffraction patterns collected during the first charge (up to 3.7 V at C/20 rate) for a $NaNi_{1/3}Mn_{1/3}Co_{1/3}O_2$ *vs.* Na cell. Corresponding voltage-composition profile is given on the right side. The inset shows an enlarged portion of the high angle region. Reprinted with permission from M. Sathiya, K. Hemalatha, K. Ramesha, J.-M. Tarascon and A. S. Prakash, *Chem. Mater.*, 2012, **24**, 1846–1853. Copyright 2012 American Chemical Society.

oxidation peak at 4.30 V. However, the NaMNCA electrode showed excellent capacity retention of 95.4% during 50 cycles. Significantly, the discharge capacity at 4.25 V was intact with only 6 mA h g^{-1} capacity loss during 50 cycles. In addition, NaMNCA could be cycled at various high rates, delivering 78, 64 and 50% of capacity at a current density of 100, 200, and 400 mA g^{-1} (Fig. 10).

Buchholz *et al.*[37] recently reported an excellent capacity retention and Coulombic efficiency of a similar composition, $Na_{0.45}Ni_{0.22}Co_{0.11}Mn_{0.66}O_2$, which is produced by treating as-synthesized $Na_{0.66}Ni_{0.22}Co_{0.11}Mn_{0.66}O_2$ powder in water. The MO_2 layer of this P2-phase is speculated to be stabilized by proton exchange into the interslab and exhibited first charge capacity of 134 mA h g^{-1} along with first discharge of 145 mA h g^{-1} within the voltage range of 2.1–4.3 V. The capacity after 275 cycles remained at 100 mA h g^{-1} which is 72% capacity retention *vs.* 2nd cycle. In addition, good high rate capabilities at 0.2 C, 0.5 C, 1 C, 2 C, and 5 C with discharge capacities of 113, 103, 94, 83, and 70 mA h g^{-1} were obtained.

The main focus regarding the layered oxides is centered on improving the stability of the materials after extensive cycling, especially at the deintercalated state, which influences the long-term stability of the crystal. In this sense, accelerating rate calorimetry (ARC) has been used to investigate the reactivity of deintercalated P2-$Na_{0.65}CoO_2$ (P2-$Na_{0.35}CoO_2$)[38] and O3-$NaNi_{0.5}Mn_{0.5}O_2$ (O3-$Na_{0.5}Ni_{0.5}Mn_{0.5}O_2$).[39] In both cases, $Na_{0.35}CoO_2$ and $Na_{0.5}Ni_{0.5}Mn_{0.5}O_2$ presented high reactivity towards the electrolyte, forming Na_xMO_2 and Co_3O_4 or $MnCO_3$ in each case, followed by O_2 evolution, which initiated solvent combustion. Both deintercalated phases reacted rapidly with $NaPF_6$ when heated in the electrolyte to form different oxides and fluorides.

Other oxides. Tepavcevic *et al.* demonstrated that electrochemically grown nanostructured bilayered vanadium pentoxide can be an efficient 3 V cathode material without the use of any carbon additive or polymeric binder.[40] The material reverts to a disordered bilayered compound after the first cycle and exhibits a stable capacity of more than 200 mA h g^{-1} at a current density of 20 mA g^{-1} after 300 cycles. Tests on the same material peeled off from the substrate show that the electrodeposition process is crucial for having a good electronic contact with the current collector and avoids capacity fading.

Hollow nanoparticles of γ-Fe_2O_3 sandwiched between carbon nanotube films have shown good cyclability with 99 mA h g^{-1} at a fast current rate of 3000 mA g^{-1} and a 99.0% coulombic for 500 cycles in the 1–4 V voltage range.[41] The charge storage mechanism is based on the sodium occupying structural defects in the hollow γ-Fe_2O_3, with a structural rearrangement of the oxygen vacancies being responsible for increase of capacity upon cycling.

Among tunnel structure oxides, there have been no relevant advances on $Na_{0.44}MnO_2$ in the last year. Only a new Ru-based phase, $Na_{2.7}Ru_4O_9$, with reversible Na de/insertion has been reported.[42]

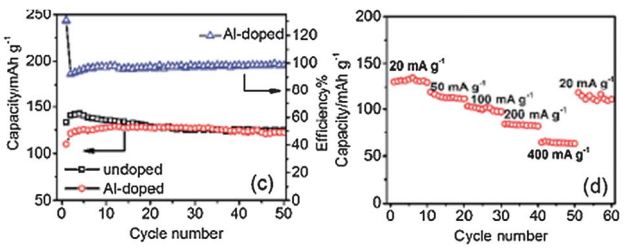

Fig. 10 Na-insertion/extraction properties of the NaMNCA microflakes: (a) cycling performance of the NaMNC and NaMNCA electrode at a constant current of 20 mA g^{-1}; (b) reversible capacities cycled at changing current rates as labelled. Reprinted with permission from C. Didier, M. Guignard, J. Darriet and C. Delmas, *Inorg. Chem.*, 2012, **51**, 11007–11016. Copyright 2012 American Chemical Society.

3.1.2 Phosphates and fluorophosphates

$NaFePO_4$. This compound is being thoroughly studied as it has the highest theoretical specific capacity among phosphate polyanion cathode materials and due to the different electrochemical behaviour compared to its Li analogue, $LiFePO_4$. Oh *et al.* prepared olivine-type $NaFePO_4$ by electrochemical delithiation of $LiFePO_4$ electrodes at a C/100 rate and their subsequent assembly in a sodium half-cell for electrochemical characterization.[43] The cells were cycled using 1 M $NaClO_4$ in a 98 : 2 volumetric mixture of PC–FEC electrolyte and a capacity value of 125 mA h g^{-1} was obtained at C/20 (80% of the theoretical capacity) with excellent capacity retention after 50 cycles. The authors observe a two-phase *plateaux* signature both upon charge and discharge although with changes in their reciprocal position, and attribute the increase in polarization with cycling to the poor ionic and electronic conductivity of $FePO_4$. Evidence of the existence of the intermediate phase $Na_{\approx 0.7}FePO_4$ both upon charge and discharge was also reported by Casas-Cabanas *et al.* from XRD data despite only one *plateau* being observed upon discharge.[44] This intermediate phase acts as a buffer to accommodate local strains that occur due to the large mismatch between the end members (17.58% in volume) and the authors attribute the different reaction path when charging or discharging the battery to the balance between interface energy penalty and mismatch between the different phases involved in the reaction. The chemical preparation of the intermediate phase $Na_{\approx 0.7}FePO_4$ revealed different types of superstructures with ordering along *a* and *b* resulting in $3a3bc$, $2a3bc$ and $a3bc$ unit cells. These superstructures are the result of different Na^+/vacancy orderings that could originate from slight differences in Na^+ content.

A comparison between the electrochemical behavior of $FePO_4$ (prepared by chemical delithiation of $LiFePO_4$) cycled *vs.* Li and *vs.* Na has been reported by Zhu *et al.* In this work it is shown that, despite the strong volumetric changes involved in the Na-ion insertion/extraction, the material is able to reversibly cycle using 1.0 M $NaClO_4$ in a EC–DMC 1 : 1 volumetric mixture for at least 100 cycles at 0.1 C with 90% of capacity retention. However, the authors attribute the worse kinetics of the sodium system to this important volumetric change in addition to the lower diffusion coefficient of Na-ion in Na_xFePO_4 and to the higher contact and charge transfer resistances when compared to its lithium counterpart.[45]

Similar capacities to those reported for crystalline olivine $NaFePO_4$ can be obtained when using amorphous $FePO_4$ nanoparticles as electroactive material electrically wired by single wall carbon nanotubes (120 mA h g^{-1} at C/10).[46] The advantage of this approach is that $FePO_4$ nanoparticles can be hydrothermally synthesized as opposed to olivine $NaFePO_4$, for which a direct synthesis has not be reported up to date because the more stable maricite polymorph is obtained instead. The authors attribute the good cycling stability (300 cycles when cycled at 2 C) to the nature of the composite as amorphous materials do not suffer from structural changes upon battery cycling while the large surface area of the composite provides improved kinetics.

$Na_3M_2(PO_4)_3$ Nasicon framework compounds. Nasicon structured compounds feature a three-dimensional framework that generates large interstitial spaces through which sodium ions can diffuse.[47–49] To be more precise, $Na_3M_2(PO_4)_3$ phases have been extensively tested and used as cathode materials for Li-ion batteries and, lately, rediscovered and studied again as electrode materials for Na-ion batteries. Especially $Na_3V_2(PO_4)_3$ displays two potential *plateaux* located at 3.4 and 1.6 V *vs.* Na/Na^+, related to the V^{3+}/V^{4+} and V^{2+}/V^{3+} redox couples, respectively. These two reaction voltages correspond to a specific capacity of 117 and 50 mA h g^{-1} for the high and low voltage zones, respectively. A recent publication by Lim *et al.* has correlated these two *plateaux* with the energies calculated for different Na distributions in the phase (Fig. 11).[50] As $Na_3V_2(PO_4)_3$ compound has two crystallographical sites for Na, they have proved that Na1 site remains totally occupied with one Na ion while Na2 site is active when the sodium content goes from $Na_3V_2(PO_4)_3$ to $NaV_2(PO_4)_3$. Moreover, they have shown that in this range, the formation of the two extreme phases is energetically favorable, so a two-phase reaction is expected. This latter point has been confirmed by *ex situ* XRD studies.

Chen *et al.* have reported the use of carbon to coat this phase by a one-step solid state reaction approach, obtaining specific capacities up to 79.5% of the theoretical one at C/20 for the high voltage *plateau*.[51] In order to improve the electrochemical behavior of this compound at high rates, a smaller particle size is needed.

The same research group has achieved higher specific capacities from $Na_3V_2(PO_4)_3$–C composites by optimizing the electrolyte used in the sodium half-cell. NaFSI/PC (sodium bis(fluorosulfonyl)amide in propylene carbonate) was selected as the optimal electrolyte system and delivered a specific capacity of 107 mA h g^{-1} at C/10 rate with 93% capacity retention after 80 cycles.[52] They have also followed the electrochemical reaction of this compound in the high voltage range by *in situ* X-ray diffraction analysis of the cathode while cycling between 2.7 and 3.7 V and it has been demonstrated that the electrochemical reaction proceeds *via* a two-phase reaction. ICP (Inductively coupled plasma) and structural analysis of this new

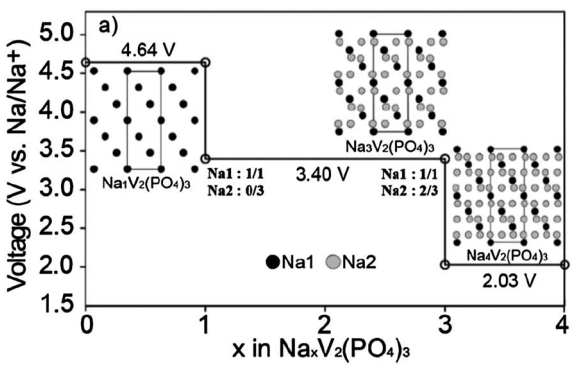

Fig. 11 Voltage profiles estimated from first principle calculations. Reproduced by permission of The Electrochemical Society from S. Y. Lim, H. Kim, R. A. Shakoor, Y. Jung and J. W. Choi, *J. Electrochem. Soc.*, 2012, **159**, A1393–A1397.

oxidized phase indicate that it corresponds to $NaV_2(PO_4)_3$ composition that retains the same structure as the sodiated phase. The diffraction peaks of this new phase obtained electrochemically are identical to those from chemically oxidized $Na_3V_2(PO_4)_3$.

A new pyro-synthesis method has recently been developed for the preparation of nanoporous, high surface area $Na_3V_2(PO_4)_3$–C composites by Kang *et al.*[53] It consists of the dissolution of the reactants in a polyol medium and the addition of an inflammable liquid thinner that provokes the self-combustion of the mixture, that is further annealed. This method produces easily materials with porous morphology of narrow pore-size distribution without the use of any template. The resulting composite displays well-developed, flat *plateaux* at 3.6 and 1.6 V *vs.* Na/Na^+ and achieves 88 mA h g^{-1} in the high voltage region at 1.33 C.

Apart from the *in situ* X-ray diffraction study made by Chen *et al.*[51] previously mentioned, Pivko *et al.* have also followed the electrochemical reaction of the vanadium Nasicon between 2 and 4 V *vs.* Na/Na^+ by *in situ* X-ray absorption spectroscopy.[54] By using a specially designed pouch cell, XANES (X-ray absorption near edge structure) results show that, during battery charge, the average V valence is gradually increased from +3 to +3.8, which is consistent with the obtained specific capacity value of 90 mA h g^{-1} (*ca.* 80% of theoretical specific capacity), this process being totally reversible. EXAFS (extended X-ray absorption fine structure) results probed the local environment of V atoms during electrochemical reaction and revealed a decrease of V–O interatomic distances in the first coordination sphere of vanadium during charge. Results obtained by both techniques indicated that the structure of $Na_3V_2(PO_4)_3$ is very rigid and stable, and that it returns to its initial state when discharged.

As was previously mentioned in the text, this Nasicon structured vanadium compound can be used both as cathode an anode, due to the two well separated potential *plateaux* displayed by the different possible vanadium redox pairs. Some years ago, Yamaki's group demonstrated that it was possible to run a symmetrical cell with this compound in both electrodes.[55] Now, they have recently published an all solid-state symmetric battery based on $Na_3V_2(PO_4)_3$ electrodes, by using $Na_3Zr_2Si_2PO_{12}$ Nasicon structured solid electrolyte.[56] They have demonstrated the viability of a novel solid-state symmetric cell fabricated by screen-printing and hot pressing. The full cell works at an average voltage of 1.8 V with an initial specific capacity of 68 mA h g^{-1} at room temperature (Fig. 12).

Although this configuration needs further optimization, such as decreasing the internal porosity of the solid electrolyte and precise control of the electrode–electrolyte interface contact, it must be said that the development of totally solid-state batteries is of great significance in terms of operation safety and cell reliability because these cells could avoid the use of conventional liquid electrolytes by using non-flammable inorganic solid electrolytes instead.

Sodium vanadium fluorophosphates ($Na_3V_2(PO_4)_2F_3$, $Na_3(VO)_2(PO_4)_2F$ and $Na_3V_2O_{2x}(PO_4)_2F_{3-2x}$). Sodium vanadium fluorophosphates are one of the main candidates for cathodic materials in Na-ion batteries, because of their high operating voltages and good specific capacity. Three different $Na_3M_2(PO_4)_2F_3$ sodium-metal fluorophosphates have been prepared and studied by Yamaki *et al.*, by using Ti, Fe and V as transition metal.[57] Among these three isostructural compounds, Ti and Fe phases presented poor electrochemical performance, but sodium-vanadium-fluorophosphate showed an excellent rate capability in sodium half cells with specific capacities up to 95 mA h g^{-1} at 4 C, displayed in two *plateaux*, at 3.65 and 4.1 V. Electrochemical tests in full cells *vs.* a $NaTi_2(PO_4)_3$ anode also exhibited very good electrochemical performance, with specific capacities of 90 mA h g^{-1} at 2 C (Fig. 13).

On the other hand, Kang *et al.* have also worked on the $Na_3V_2(PO_4)_2F_3$ phase.[58] They have confirmed the structure proposed by Le Meins *et al.*[59] for this compound by neutron diffraction. *Ex situ* structural study of cycled electrodes indicated that the electrochemical process consists of a one-phase reaction, implying topotactic Na extraction/insertion with an average volume change of 1.8%, which can be the key for a long and good cyclability for this material. First principle investigations about the voltage of the electrochemical reaction from $Na_3V_2(PO_4)_2F_3$ to $Na_1V_2(PO_4)_2F_3$ resulted in an average voltage of 3.8 V *vs.* Na/Na^+, which is in good agreement with experimental data. Moreover, theoretical calculations led to proposing that the electroactive redox pair in this phase is V^{3+}/V^{4+}.

The V^{4+} $Na_3(VO)_2(PO_4)_2F$ phase has demonstrated that this compound is able to extract and insert reversibly Na^+ ions *vs.* a metallic sodium anode in two reaction voltages, 3.6 and 4.0 V.[60]

A recent work by our group has established for the first time a relationship between $Na_3V_2(PO_4)_2F_3$ and $Na_3(VO)_2(PO_4)_2F$ fluorophosphates. These compounds possess the same framework with one fluorine atom replaced by an oxygen, thus forming a family of the general formula $Na_3V_2O_{2x}(PO_4)_2F_{3-2x}$ where $0 \leq x \leq 1$ (ref. 61) (Fig. 14). The end members of this family correspond to the mentioned phases with +3 and +4 oxidation states for vanadium, respectively, while a set of new

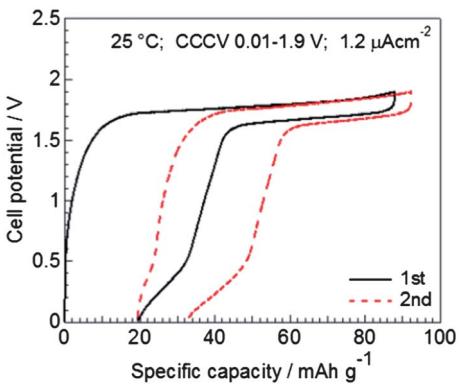

Fig. 12 Charge/discharge profiles of the symmetric all solid-state cell at 1.2 mA cm^{-2} between 0.01 and 1.9 V at room temperature. Reprinted from Y. Noguchi, E. Kobayashi, L. S. Plashnitsa, S. Okada and J.-I. Yamaki, Fabrication and performances of all solid-state symmetric sodium battery based on NASICON-related compounds, *Electrochim. Acta*, DOI: 10.1016/j.electacta.2012.11.038, in press. Copyright 2013, with permission from Elsevier.

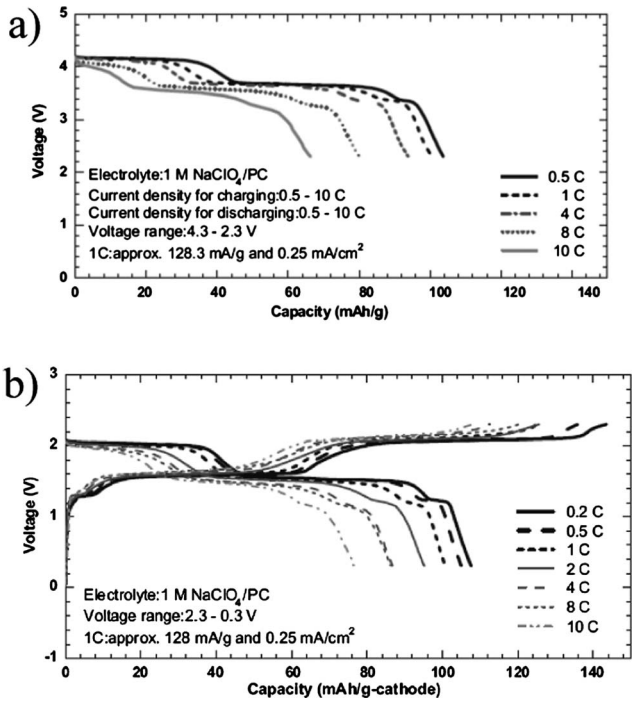

Fig. 13 Discharge capacity of $Na_3V_2(PO_4)_2F_3$ cathode at different current rates (a) in half cell *vs.* Na/Na^+ (b) in full cell with $NaTi_2(PO_4)_3$ as anode. Reprinted from K. Chihara, A. Kitajou, I. D. Gocheva, S. Okada and J.-I. Yamaki, Cathode properties of $Na_3M_2(PO_4)_2F_3$[M = Ti, Fe, V] for sodium-ion batteries, *J. Power Sources*, 2012, **227**, 80–85. Copyright 2012, with permission from Elsevier.

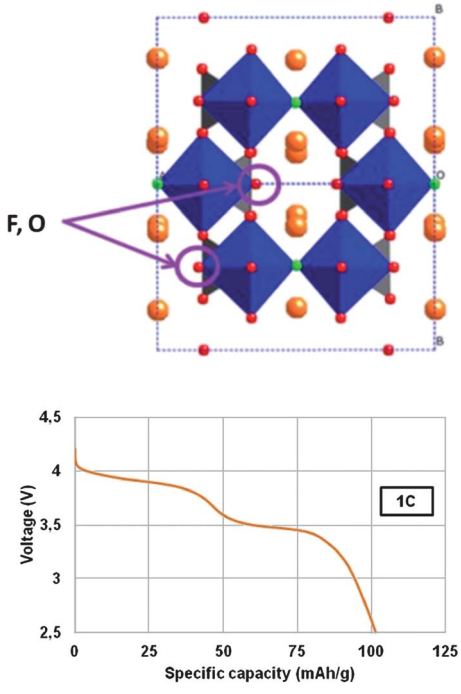

Fig. 14 (a) Structure of mixed-valence $Na_3V_2O_{2x}(PO_4)_2F_{3-2x}$ family. Marked sites can be occupied either by F or O atoms; and (b) discharge profile and specific capacity of a mixed-valence $Na_3V_2O_{2x}(PO_4)_2F_{3-2x}$ sample.

intermediate compositions with mixed vanadium valence have been prepared.

Because of the similar scattering factors of V^{3+} and V^{4+} and O^{2-} and F^-, the different members of this family of compounds cannot be distinguished by X-ray diffraction and magnetic measurements have been used instead, which was revealed in this work to be crucial. The attainment of the different compositions is related to the carbon content in the samples. This carbon, added to the precursor in different proportions, plays a protective role in the VPO_4 precursor during the hydrothermal process and hinders the complete oxidation of V^{3+} to V^{4+}. It has been demonstrated that the presence of a moderate carbon percentage and thus, a mixed valence in the samples enhances the electrochemical performances with specific capacities of 100 mA h g^{-1} at 1 C.[61]

The electrochemical behaviour of this mixed-valence family of compounds, with the same voltage *plateaux* for the V^{4+} end member and the mixed-valence samples (3.65 and 4.1 V *vs.* Na/Na^+), led to proposing a tentative mechanism where the redox reaction taking place would correspond to the V^{4+}/V^{5+} pair.

$$\text{Charge: } Na_3(VO)_2(PO_4)_2F \rightarrow Na(VO)_2(PO_4)_2F + 2Na^+ + 2e^- \quad (1)$$

$$\text{Discharge: } Na(VO)_2(PO_4)_2F + 2Na^+ + 2e^- \rightarrow Na_3(VO)_2(PO_4)_2 \quad (2)$$

Rate capability of this mixed valence material ranges from specific capacities of 100 mA h g^{-1} at C/20 to 75 mA h g^{-1} at 5 C. Cycling stability at 1 C showed coulombic efficiency higher than 99% and capacity retention of 95% after 200 cycles[62] (Fig. 15).

If all electrochemical performances of the compounds presented in this section are compared, it can be seen that all of them react at two voltage steps of very similar values: 3.6 and 4.1 V *vs.* a sodium anode. In order to clarify which is the redox couple in each case, it is necessary to carry out a deep study of the electrochemical mechanism taking place during sodium extraction/insertion in all these systems: $Na_3V_2(PO_4)_2F_3$, $Na_3(VO)_2(PO_4)_2F$ and $Na_3V_2O_{2x}(PO_4)_2F_{3-2x}$, including an analysis of the vanadium oxidation state in each point of the charge/discharge.

Sodium iron-manganese fluorophosphates (Na_2FePO_4F, Na_2MnPO_4F and $Na_2(Fe,Mn)PO_4F$). Among the possible fluorophosphate materials, Fe and Mn compounds present different structures due the difference in ionic radii between Fe^{2+} and Mn^{2+} (0.61 and 0.81 Å in octahedral coordination, respectively). Whereas the sodium-iron fluorophosphate possesses a two-dimensional layered structure,[63] the sodium-manganese fluorophosphate presents a three-dimensional tunnel structure[64] (Fig. 16). This fact leads to different electrochemical properties. The iron phase, on the one hand, is able to exchange one electron at *ca.* 3.0 V *vs.* Na/Na^+, distributed in two close *plateaux* with an intermediate $Na_{1.5}FePO_4F$ phase that presents intermediate lattice parameters between the two end members and *P*2/*c* monoclinic symmetry. On the other hand, the manganese compound has demonstrated to be poorly electrochemically active.[65] For that reason, literature is more extensive for the iron compound, the manganese remaining as a

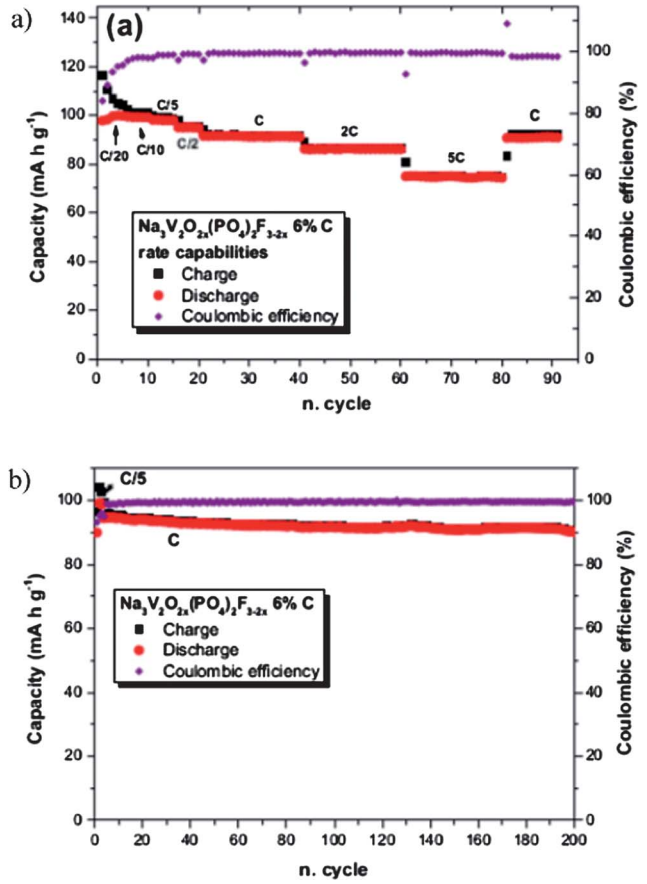

Fig. 15 (a) Specific charge/discharge capacity of $Na_3V_2O_{2x}(PO_4)_2F_{3-2x}$ at different C rates; and (b) cycling stability of $Na_3V_2O_{2x}(PO_4)_2F_{3-2x}$ over 200 cycles with a charge/discharge rate of C. The first 3 cycles were recorded with C/5. Reprinted from P. Serras, V. Palomares, A. Goñi, P. Kubiak and T. Rojo, Electrochemical performance of mixed valence $Na_3V_2O_{2x}(PO_4)_2F_{3-2x}$/C as cathode for sodium-ion batteries, *J. Power Sources*, 2013, **241**, 56–60. Copyright 2013, with permission from Elsevier.

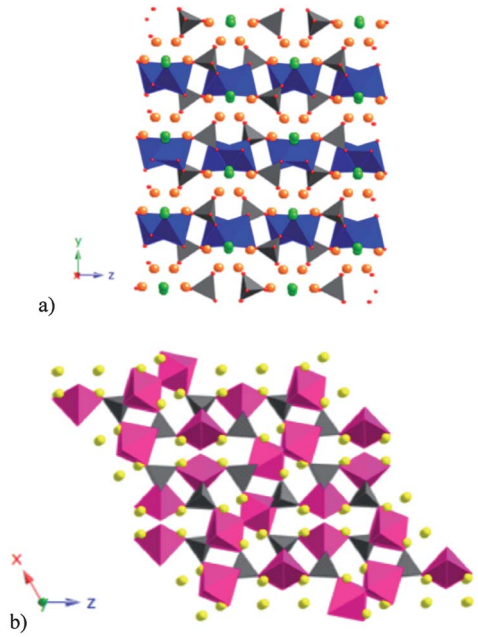

Fig. 16 Structures of (a) Na_2FePO_4F and (b) Na_2MnPO_4F.

dopant in this latter phase, with the aim of achieving higher potentials.

Na_2FePO_4F was prepared by solid state synthesis by Komaba *et al.* using ascorbic acid as the carbon source in order to control the particle size and get a carbon coating around the active phase particles.[66] In this way, the resulting composite with 1.3% wt carbon was able to deliver 110 mA h g^{-1}, 90% of its specific capacity (124 mA h g^{-1}) at C/18 in two close *plateaux*, at 3 and 2.9 V *vs.* Na/Na^+. The rate capability tests with charging at C/20 and discharging at 1 C displayed a discharge capacity of 60 mA h g^{-1} (about 50% of its specific theoretical capacity). The 2 wt% carbon coating on the active particles demonstrated to have a huge effect on the electrochemical performance of this phase, raising the discharge specific capacity at C/20, as can be seen in Fig. 17.

A recent publication by Langrock *et al.* has shown improved performance with respect to the results shown above by using a different strategy on the preparation of Na_2FePO_4F material, by building carbon coated porous, hollow spheres of the active material by ultrasonic spray pyrolysis.[67] This nanostructured material (Fig. 18) presents a 500 nm average diameter (from 100 nm to 1 μm) and 80 nm wall thickness, with micro-sized cavities and nanopores inside the outer wall of about 2.5 nm size. This composite, that contains about 6–8% wt carbon, presents a specific surface of 8.7 m^2 g^{-1}. Electrochemical extraction/insertion of Na in this composite takes place in the two *plateaux* typical of Na_2FePO_4F at 3.1 and 2.9 V and displays a specific capacity of 90 mA h g^{-1} at C/10 and demonstrates good cycling stability for 100 cycles, probably due to its remarkable morphology. The material presented in this work displays good rate capability and one of the longest cycling stabilities reported for this compound. The large reaction area and interior void space that accommodates the volume changes during redox reaction, lead to enhanced reaction kinetics and cycling stability of the material.

When iron is partially substituted by manganese in the formula $Na_2Fe_{1-x}Mn_x(PO_4)F$, the layered structure is conserved up to $x = 0.1$, and three-dimensional tunnel structure appears in the range $0.3 < x < 1$, as has been demonstrated by Wu *et al.*[68] Komaba *et al.* have demonstrated that a 3-D structure $Na_2Fe_{0.5}Mn_{0.5}PO_4F$–C composite displays 110 mA h g^{-1} at C/20 rate in three voltage regions, the two typical of the iron fluorophosphates, and another one, assigned to Mn^{2+}/Mn^{3+} redox pair at 3.53 V.[69] The rate capability of this compound was also better as compared to the iron phase, maintaining 70% of its reversible capacity when going from C/20 to 1 C rate.

On the other hand, a recent report by Kim *et al.* shows that carbon coated Na_2MnPO_4F material can offer a 120 mA h g^{-1} specific capacity at C/12.5 rate at room temperature, which corresponds almost to the theoretical capacity for the exchange of 1 Na^+ ion.[70] The extraction of a second Na^+ has also been observed at 4.67 V *vs.* Na/Na^+. Although this compound showed

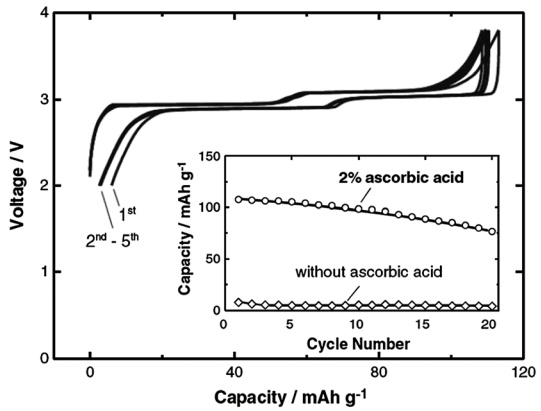

Fig. 17 Galvanostatic charge/discharge curves of a Na/Na_2FePO_4F cell cycled at C/20 rate. Inset: capacity retention of a carbon coated and carbon free samples. Reprinted from Y. Kawabe, N. Yabuuchi, M. Kajuyama, N. Fukuhara, T. Inamasu, R. Okuyama, I. Nakai and S. Komaba, Synthesis and electrode performance of carbon coated Na_2FePO_4F for rechargeable Na batteries, *Electrochem. Commun.*, **13**, 1225–1228. Copyright 2011, with permission from Elsevier.

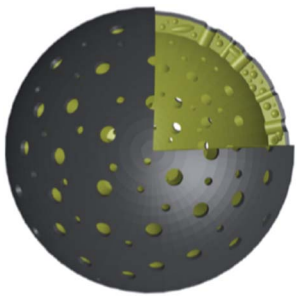

Fig. 18 Scheme of a porous hollow Na_2FePO_4F/C particle. Reprinted from A. Langrock, Y. Xu, Y. Liu, S. Ehrman, A. Manivannan and C. Wang, Carbon coated hollow Na_2FePO_4F spheres for Na-ion battery cathodes, *J. Power Sources*, 2013, **223**, 62–67. Copyright 2013, with permission from Elsevier.

poor capacity retention and significant polarization, these are the best results registered to date for Na_2MnPO_4F phase *versus* a sodium anode.

Pyrophosphates. Among the phosphates family, pyrophosphates have recently been pointed out as possible electroactive materials to be used as cathodes for Na-ion batteries. Pyrophosphate compounds offer a robust and stable three-dimensional $(P_2O_7)^{4-}$ framework with multiple sites for alkali ions. Moreover, the abundance of structural configurations for these compounds leads to a very rich set of possible scaffolds for Na ion insertion or extraction. In a recent publication, Yamada's group has gathered a large group of possible cathodic materials based on pyrophosphate anion[71] that are shown in Table 1 with their calculated specific capacity.

As can be observed in Table 1, theoretical specific capacity values are close to 100 mA h g^{-1} but only exceed this figure in two cases, for the Fe and Mn phases, the latter being the only one that could exchange more than one electron per formula due to the possible oxidation states of the transition metals and the availability of space for the insertion of more Na^+ ions. This way, it can be said that, in general, pyrophosphate-based compounds present as advantage their great stability and versatile structures, but exhibit low theoretical specific capacities, due to the larger weight of pyrophosphate anion compared to normal phosphates or, even oxides.

Despite this disadvantage, these compounds are being studied in Na-ion battery field, specially, $Na_2FeP_2O_7$, due to the low price of all its components. This compound, that presents a triclinic structure with $P\bar{1}$ space group, is isostructural to $Na_2CoP_2O_7$,[72] and presents multidimensional open Na^+ channels (Fig. 19).

Non-coated, micron sized $Na_2FeP_2O_7$ particles (3–5 μm) have shown a discharge capacity of 82 mA h g^{-1} at C/20, 97 mA h g^{-1} being its theoretical specific capacity (Fig. 20). The charge–discharge curves of this compound present two electroactive zones: a small *plateau* at 2.5 V, and a larger one at *ca.* 3 V that consists of three small steps. Very small volume shrinkage of 2.1% was observed during Na removal which could provide a very good stability during cycle life.[73]

Choi *et al.* have also focused their attention on this compound, and have recently published a deeper study on its electrochemical behavior and mechanism.[74] They have prepared carbon coated particles of $Na_2FeP_2O_7$ and have studied the electrochemical curves of this phase, comparing the results with theoretical calculations (Fig. 21). They observe that there are 3 sets of Na sites in the structure that can be linked to the different zones in the charge–discharge curves. The 2.5 V *plateau* would be related to a single phase reaction that implies the filling of Na1 sites during a first period of discharge, and the reactions taking place around 3 V would be linked to several two-phase reactions going through various intermediate phases. The calculated reaction voltages for this system agree well with the ones observed by cyclic voltammetry. This compound demonstrates to be stable up to 550 °C, which represents great thermal stability.

Komatsu *et al.* have recently prepared a family of glass–ceramics with the formula $Na_{2-x}Fe_{1+x/2}P_2O_7$ ($0 < x < 0.44$) by a melt-quenching method.[75] They have also observed a main voltage *plateau* at 2.9 V and a shorter one at 2.5 V *vs.* Na/Na^+. The specific capacities of these compounds range from 86 mA h g^{-1} at C/20 to 45 mA h g^{-1} at 10 C.

Another possible family of materials is the mixed phosphate–pyrophosphates, such as $Na_4Fe_3(PO_4)_2(P_2O_7)$, that has been studied by Kang *et al.*[76] due to the great stability that offer both phosphate and pyrophosphate frameworks and the low

Table 1 Possible pyrophosphate compounds considered by Barpanda *et al.* and their calculated theoretical specific capacity[71]

Compound	Theoretical C_{sp} (mA h g^{-1})
$NaFeP_2O_7$	106.04 (1 inserted Na)
$Na_2CoP_2O_7$	96.12 (1 extracted Na)
$Na_2MnP_2O_7$	195.05 (2 extracted Na)
$Na_2CuP_2O_7$	94.56 (1 inserted Na)
$Na_2VOP_2O_7$	93.44 (1 extracted Na)

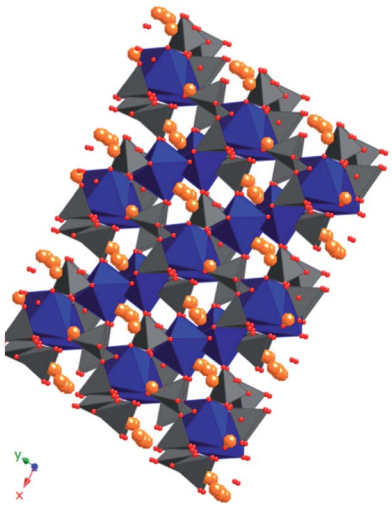

Fig. 19 Structure of $Na_2FeP_2O_7$ compound.

price and great abundance of Fe in nature. The resulting $Na_4Fe_3(PO_4)_2(P_2O_7)$ phase exhibits a theoretical specific capacity of 129 mA h g^{-1} for 3 Na^+ ions exchange and has demonstrated to operate at 3.2 V *vs.* a sodium anode and to discharge about 100 mA h g^{-1} at C/20 rate. The strong framework made up of phosphate and pyrophosphate anions makes this compound very stable (Fig. 22), even in its oxidized state, up to 500 °C, as has been observed in DSC measurements. The small volume change during redox reaction, of about 4%, is a good sign for future long-term cycling and cycle life tests. Although deeper studies must be done about this phase, existing work shows that this material is promising in terms of operating voltage and high specific capacity.

A recently published article by Park *et al.* describes the preparation of a new triclinic polymorph of $Na_2MnP_2O_7$ phase ($P\bar{1}$) that presents unexpected electrochemical activity.[77] Polyanion manganese-based compounds (pyrophosphates, phosphates, *etc.*) usually suffer from far inferior electrochemical performance originating from low electronic conductivity and poor mobility of the phase boundary, which are directly related to Jahn–Teller distortion of Mn^{3+} as well as large lattice mismatch between the charged and discharged states.[78–80] For this reason, the achievement of a reversible specific capacity value of 90 mA h g^{-1} at C/20 at room temperature, which represents 92% of the theoretical specific capacity value is described as anomalous by the authors.

In this work, they explain on a DFT calculation basis (density functional theory) how the different structure of the new $Na_2MnP_2O_7$ phase, consisting of a Mn–O polyhedron sharing edges directly with the neighbouring one affects the kinetics of the reaction and the electrochemical response of the material. The calculated reaction potentials agree with the three operation voltages observed between 1.5 and 4.5 V *vs.* Na/Na^+ in the cyclic voltammetry measurements (Fig. 23), and *ex situ* XRD analysis of the cycled cathodes indicates that the fully charged state corresponds to the extraction of one Na^+ ion from the structure.

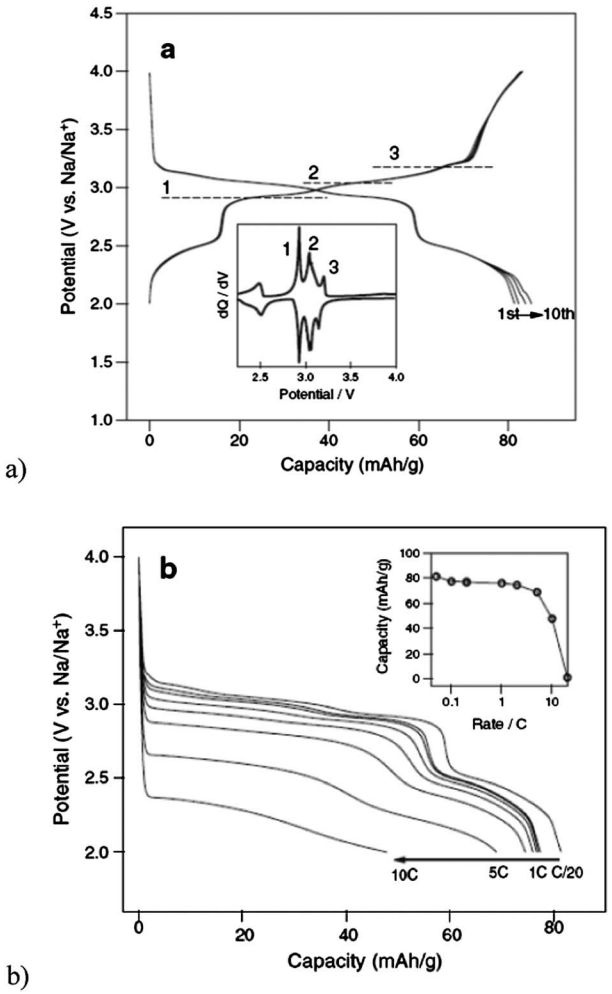

Fig. 20 (a) Galvanostatic voltage-composition curve at C/20 and (b) discharge capacity of $Na_2FeP_2O_7$ at different rates. Reprinted from P. Barpanda, T. Ye, S.-I. Nishimura, S.-C. Chung, Y. Yamada, M. Okubo, H. Zhou and A. Yamada, Sodium iron pyrophosphate: A novel 3.0 V iron-based cathode for sodium-ion batteries, *Electrochem. Commun.*, 2012, **24**, 116–119. Copyright 2012, with permission from Elsevier.

The new electroactive polymorph presents good cycling stability, retaining 96% of the initial specific capacity for 30 cycles at C/5. This work suggests the possible existence of other polymorphic structures for unreported transition metal species with unexpected electrochemical properties, as for $Na_2MnP_2O_7$.

Other cathodic materials. The bigger size of Na^+ ions compared to Li^+ has driven research interest also towards open host frameworks with a large interstitial space, such as Prussian Blue derivatives containing a suitable transition-metal to support reversible Na insertion/extraction. In this sense, Goodenough *et al.* have investigated the electrochemical properties of two compound families: $KMFe(CN)_6$ where M can be Mn, Fe, Co, Ni or Zn;[81] and $Na_xMnFe(CN)_6$.[82] These compounds present the advantage of being easily synthesized in a solution method from low-cost cations. Although some of them have already been tested as electrodes for aqueous batteries (see section 2), this fact limits the stable voltage window of the

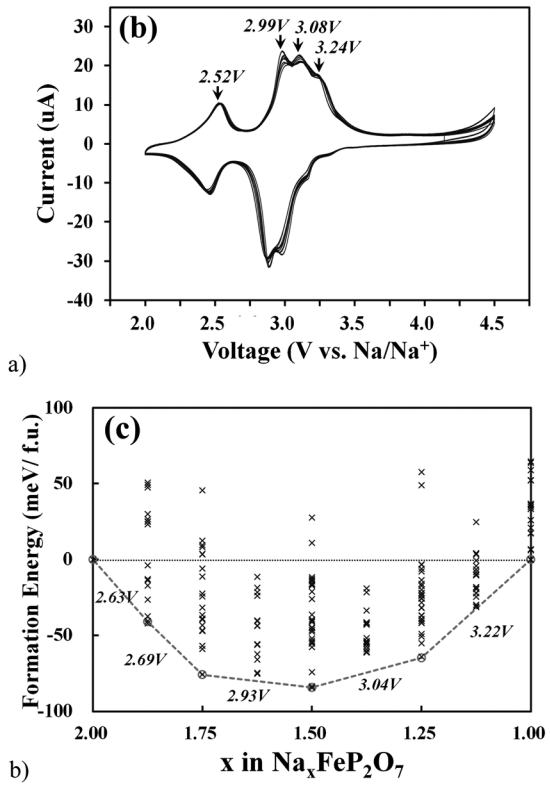

Fig. 21 (a) Cyclic voltammetry of $Na_2FeP_2O_7$ with electrochemical reaction potentials and (b) calculated formation energy hull and potentials for consecutive compositional intervals. Reprinted from H. Kin, R. A. Shakoor, C. Park, S. Y. Lim, J.-S. Kim, Y. N. Jo, W. Cho, K. Miyasaka, R. Kahraman, Y. Jung and J. W. Choi, $Na_2FeP_2O_7$ as a Promising Iron-Based Pyrophosphate Cathode for Sodium Rechargeable Batteries: A Combined Experimental and Theoretical Study, *Adv. Funct. Mater.*, **23**, 1147—1155. Copyright 2013, with permission from Wiley.

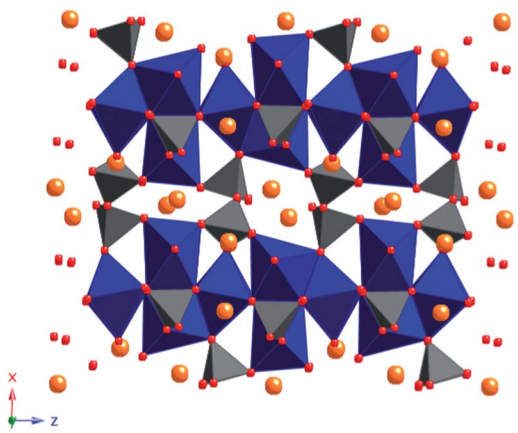

Fig. 22 Structure of $Na_4Fe_3(PO_4)_2(P_2O_7)$.

battery to 1.5 V, so research has been extended to non-aqueous electrolytes based on a sodium salt ($NaClO_4$ or $NaPF_6$) saturated in an EC : PC (1 : 1) solution (ethylene carbonate : propylene carbonate).

$KFe(II)Fe(III)(CN)_6$ Prussian Blue analogue exhibited a reversible capacity of about 65 mA h g^{-1} at C/20 for 30 cycles

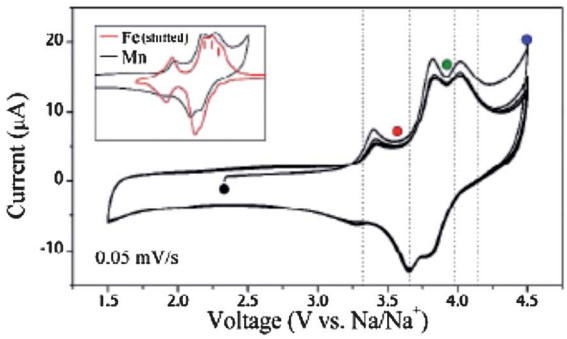

Fig. 23 CV profile of $Na_2MnP_2O_7$ new polymorph. Reprinted with permission from C. S. Park, H. Kim, R. A. Shakoor, E. Yang, S. Y. Lim, R. Kahraman, Y. Jung and J. W. Choi, *J. Am. Chem. Soc.*, 2013, **135**, 2787–2792. Copyright 2013 American Chemical Society.

at room temperature, maintaining more than 99% of the initial specific capacity.[81] Low coulombic efficiency was registered in the first cycles due to residual water in the lattice. The moderate specific capacity and good reversibility of this material motivated further research on this kind of structures by exchanging Na^+ for K^+, leading to two sodium manganese hexacyanoferrates with different structures, rhombohedral $Na_{1.72}MnFe(CN)_6$ and cubic $Na_{1.4}MnFe(CN)_6$.[82] Different structures and M–CN bonding in both compounds led to different open circuit voltages, reversible capacity and cycling performance. Both materials presented reversible specific capacities higher than 120 mA h g^{-1} at C/20 rate at room temperature (Fig. 24). Rhombohedral sodium manganese hexacyanoferrate presented fast capacity fade for the first 10 cycles, but then stabilized, whereas the cubic one showed negligible capacity fade for 30 cycles. Both electrodes demonstrated to be very stable during cycling, because no Mn or Fe dissolution was observed in the high current cycled cell electrolyte. The rhombohedral compound showed excellent rate capability up to a high discharge rate of 40 C. The latter feature can compensate for the lower specific capacity of this family of compounds as compared to Li-based battery electrodes, by enhancing the power density of the Na-ion battery.

Polymeric electrodes are also being studied as possible cathodes for Na-ion batteries. Within this category, p-type electroactive polymers have potentially high redox capacity and flexible host matrixes for a doping–dedoping reaction of anions, irrespective of the nature of cations. Zhao *et al.* have reported an aniline/*o*-nitroaniline copolymer (P(AN-NA)) with high redox capacity and stable cyclability in $NaPF_6$ based electrolyte.[83] This material shows two pairs of broad redox bands in cyclic voltammetry *vs.* Na/Na^+ at 3.75/3.5 V and 3.15/2.65 V, which is very similar to the electrochemical response of PAN electrodes in organic Li-ion battery electrolytes. Galvanostatic cycling of this copolymer showed a specific capacity over 173 mA h g^{-1} for 50 cycles at an average working potential of ~3.2 V in coin cells *vs.* Na/Na^+.

Fig. 25 shows electrochemical profiles of the studied electrode at different current rates and its rate capability (inset). As

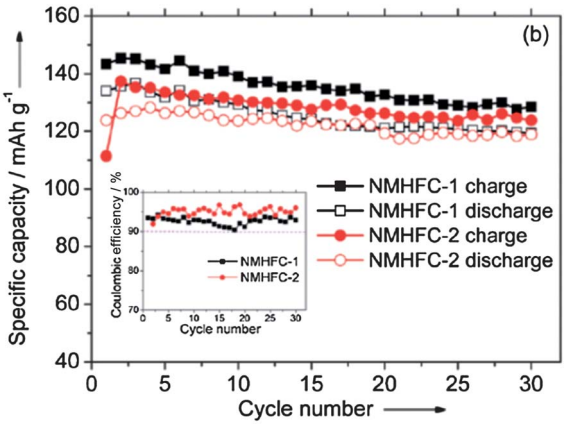

Fig. 24 Charge/discharge capacity and coulombic efficiency (inset) *vs.* cycle number of rhombohedral $Na_{1.72}MnFe(CN)_6$ and cubic $Na_{1.4}MnFe(CN)_6$. Reprinted from L. Wang, Y. Lu, J. Liu, M. Xu, J. Cheng, D. Zhang and J. B. Goodenough, A Superior Low-Cost Cathode for a Na-Ion Battery, *Angew. Chem., Int. Ed.*, 2013, **52**, 1964–1967. Copyright 2013, with permission from Wiley.

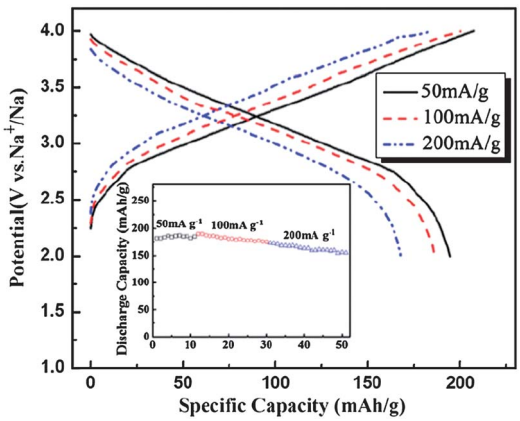

Fig. 25 Electrochemical profiles of the P(AN-NA) electrode at different current rates and its rate capability (inset). Reprinted from R. Zhao, L. Zhu, Y. Cao, X. Ai and H. X. Yang, An aniline-nitroaniline copolymer as a high capacity cathode for Na-ion batteries, *Electrochem. Commun.*, 2012, **21**, 36–38. Copyright 2012, with permission from Elsevier.

can be seen, this electrode demonstrates to have good rate capability and strong cyclability that result from the flexibility of the polymer matrix which minimizes size restrictions. These features can be essential for the development of Na-ion batteries, which usually suffer from poor rate capabilities due to the difficult transport of large size Na^+ ions in inorganic lattices.

Zhou *et al.* have developed a strategy to improve the capacity of the polymeric materials. This strategy consists in immobilizing redox-active anions into the electroactive polymer chains by incorporating large anionic redox species that can contribute their redox capacity to the materials and provoke combined redox processes along with cationic insertion/extraction reactions. They produced a diphenylamine-4-sulfonate-doped polypyrrole [$C_{12}H_{10}NSO_3^-$-doped $(C_4H_3N)_n$, Ppy/DS] where the large anionic counterions can activate the electronic conduction and the electrochemical activity of the polymer network, and also can serve as active redox sites for reversible Na storage.[84]

The electrochemical activation effect was observed in the cyclic voltammetry curve (Fig. 26), where a quasi rectangle capacitive band from the Ppy fraction is appreciated, with two pairs of peaks at 3.7 and 2.5 V, corresponding to a synergistic redox reaction of the diphenylamine-4-sulfonate anions and Ppy chains.

This organic–polymer composite showed a specific capacity of 115 mA h g^{-1} with good cycling stability (82% capacity retention for 50 cycles) and convenient rate capability at 50 mA g^{-1}. The easiness of the chemical doping process can make it possible to extend it to a large variety of organic anions and polymer networks, opening a path for low cost electrochemically active polymer cathodes for energy storage applications.

Finally, $AMSO_4F$ materials where A is an alkali and M a transition metal, must be mentioned as possible electrodes for sodium-ion batteries.[85] Not much work has been done in this direction, but J. M. Tarascon *et al.* have recently pointed out that $FeSO_4F$ framework obtained from electrochemically oxidized $KFeSO_4F$ was able to insert and extract up to 0.85 Na^+ ions into its structure at *ca.* 3.5 V *vs.* a metallic sodium anode in a two step process with very low polarization. This feature makes fluorosulfates possible electrodes for Na-ion systems .

A summary of the most relevant cathode systems discussed in this section, together with their reported capacity and voltage, can be found in Table 2.

3.2 Anodes

While in the field of cathode materials the replacement of lithium by sodium has been a common route for finding good electrodes, the inability of sodium to insert into graphite, and the up-to-now uncertain formation of a stable SEI layer is hindering the advance towards preparing full sodium ion

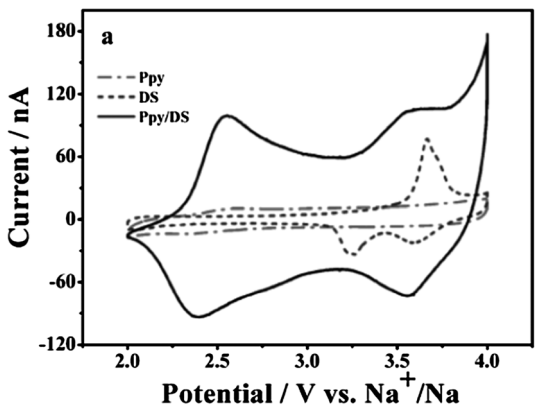

Fig. 26 Comparison of the electrochemical behavior of polypyrrole, diphenylamine-4-sulfonate, and diphenylamine-4-sulfonate-doped polypyrrole *vs.* Na/Na^+. Reprinted from M. Zhou, Y. Xiong, Y. Cao, X. Ai and H. Yang, Electroactive organic anion-doped polypyrrole as a low cost and renewable cathode for sodium-ion batteries, *J. Polym. Sci., Part B: Polym. Phys.*,2013, **51**, 114–118. Copyright 2013, with permission from Wiley.

batteries. In fact the most recent advances of anode material for Na-ion batteries have been mainly accompanied by the use of electrolyte additives or more stable binder compositions, while full sodium cells have mainly made use of $NaTi_2(PO_4)_3$ as anode material, despite its sodium insertion occurring at voltages as high as 2.0 V *vs.* Na^+/Na. Therefore development of anode materials and electrolyte compositions must happen simultaneously.

3.2.1 Recent approaches with carbons based materials. *Hard carbons* remain the main candidate to be used as anode for sodium ion batteries, although their performance is still far from that achieved by graphite in lithium-ion batteries. Recent approaches to improve its cyclability have been the use of hierarchically porous carbons prepared by templating routes. The electrochemical response of these materials, measured in 3 electrode beaker cells, showed a huge irreversible first cycle capacity, but it was able to deliver more than 100 mA h g^{-1} at 5 C with good coulombic efficiency after several cycles.[86] On the other hand, Komaba *et al.*, worked not on the material itself but on the optimization of the electrolyte composition, solvents and salts, as well as the low voltage cutoff.[87] They conclude that 1 M $NaClO_4$ in PC (propylene carbonate) or EC (ethylene carbonate) or EC : DEC (ethylene carbonate : diethyl carbonate) electrolyte compositions result in better performance with respect to mixtures of the same salt in BC (butylene carbonate), EC : DMC (ethylene carbonate : dimethyl carbonate) or EC : EMC (ethylene carbonate : ethyl methyl carbonate); achieving an optimized capacity as high as 240 mA h g^{-1} for more than 100 cycles at C/10 when cycling down to 0 V. Additionally, in an attempt to improve the stability of the SEI layer they found that the use of VC (vinilydene carbonate), a conventional electrolyte additive for LIB has a detrimental effect on the performance. A detailed investigation on the electrolyte optimization based on the study of electrolyte viscosity, ionic conductivity, thermal stability and potential window stability was performed by Ponrouch *et al.*[88] In this work they conclude that $NaPF_6$ in PC alone seems the more appropriate electrolyte for generic sodium ion batteries with respect to $NaClO_4$ or NaTFSI (sodium trifluoromethane sulfonate) salts in carbonate, glymes, glycols and their mixtures, however when it comes to hard carbon, EC : PC mixtures are preferred. Moreover, Ponrouch *et al.* have recently shown that in the case of hard carbon prepared from the pyrolysis of sugar, the addition of 2% wt FEC to 1 M $NaClO_4$ in EC : PC additive has detrimental effects, due to the formation of a less conducting SEI layer, as shown by impedance measurements in three electrode cells.[89] Besides, capacity as high as 300 mA h g^{-1} is reversibly obtained at C/10 for more than 100 cycles in 2 electrode cells cycled between 0 and 2.0 volts by optimization of HC (hard carbon) processing.

Carbon based hollow nanowires[90] *and hollow nanospheres*[91] show improved specific sodium insertion with respect to their solid counterparts, due to a more efficient sodium diffusion within the material as shown in Fig. 27. While the hollow nanospheres showed 200 mA h g^{-1} reversible capacity for 100 cycles at 50 mA g^{-1} in 1 M $NaClO_4$ in PC in the voltage range 0.001–3.0 V, the hollow nanotubes deliver 250 mA h g^{-1} reversible capacity at the same current of 50 mA g^{-1} but over a narrower voltage range 1.2–0.01 V *vs.* Na/Na^+ with 82% capacity retention for 400 cycles. The good cyclability is attributed to the short diffusion distance that sodium ions need to travel in the hollow carbon and the quite large average graphitic interplanar distance in the as prepared nanowires. Interestingly it delivers 150 mA h g^{-1} at a high rate of 500 mA g^{-1} in 1 M $NaClO_4$ in EC : EMC.

More recently, reduced graphene oxide (RGO), which can be produced in large quantities by cheap methods, has shown an intermediate performance between that of hollow nanotubes and nanospheres in the same electrolyte, with a reversible capacity of 177 mA h g^{-1} at 200 mA g^{-1} and a capacity of 93 mA h g^{-1} after 1000 cycles (Fig. 28).[92]

Table 2 Summary of the most relevant cathode systems, together with their reversible capacities and average operating voltages for sodium-ion batteries[a]

Compound	Reversible C_{sp} (mA h g^{-1})	Average operating voltage *vs.* Na/Na^+ (V)	Reference
P2-$Na_x[Fe_{1/2}Mn_{1/2}]O_2$	190	~2.75	18
O3-$Na[Ni_{1/3}Fe_{1/3}Mn_{1/3}]O_2$	100	2.75	32 and 33
$Na_{0.44}MnO_2$	160	~2.75	
$Na_{0.45}(Mn_{0,66}Ni_{0,22}Co_{0,11})O_2$	141	2.3, 3.65, 4.25	35
$NaFePO_4$	154	~2.9	43 and 44
$Na_3V_2(PO_4)_3$	50	1.6	50
	117	3.5	
$Na_3V_2O_{2x}(PO_4)_2F_{3-2x}$	130	3.6 and 4.1	61 and 62
$Na_3V_2(PO_4)_2F_3$	130	3.6 and 4.1	57
Na_2FePO_4F	124	2.9–3	66
Na_2MnPO_4F	125	~3.66	70
$Na_2FeP_2O_7$	97	2.5 and 3.2	73
$Na_2MnP_2O_7$	98	~3.5	77
Prussian blue analogues	~200	~3.3	82
Polymeric cathodes	~173	~3.2	83
$NaFeSO_4F$	138	3.5	85

[a] Exp: experimental.

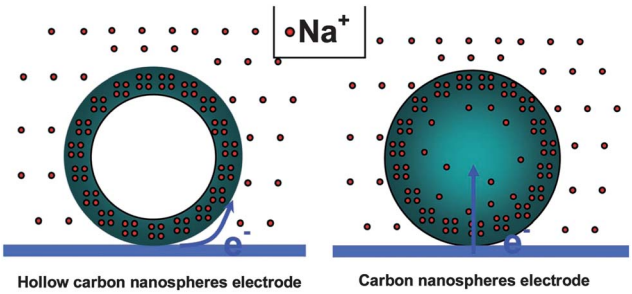

Fig. 27 Schemes of the electrochemical reaction process of hollow carbon nanospheres and solid carbon spheres. Reprinted from Y.-X. Wang, S.-L. Chou, H.-K. Liu and S.-X. Dou, Reduced graphene oxide with superior cycling stability and rate capability for sodium storage, *Carbon*, 2013, **57**, 202–208. Copyright 2013, with permission from Elsevier.

N-doped carbonaceous materials are commonly studied while tailoring the electrical and electrochemical properties of materials. Interconnected nanofibres produced from annealing polypyrrole can deliver reversible capacity higher than 130 mA h g^{-1} at a current density of 200 mA g^{-1} for 200 cycles and 73 mA h g^{-1} at a high current density of 20 A g^{-1} between 0.1 and 2.0 V.[93] This behaviour, observed in 1 M $NaPF_6$ EC : DEC : PC is close to that of supercapacitors, which is probably due to the surface redox phenomena being major rather than bulk processes. Polypyrrole has also been the precursor for the synthesis of N-doped carbon nanosheets,[94] which in 1 M $NaPF_6$ EC : DMC delivered larger capacity than the nanofibres at low currents, ~300 mA h g^{-1} at 50 mA g^{-1}, but only 50 mA h g^{-1} at 20 A g^{-1}. Nevertheless the capacity retention in 10 cycles is less than 70%.

3.2.2 Titanates. With potentials for sodium insertion larger than those of carbon, sodium plating can be avoided in titanates, which makes them also promising candidates for anodes in sodium-ion batteries. Since the reversible insertion of 2 sodium ions in $Na_2Ti_3O_7$ was shown to occur at a voltage as low as 0.3 V *vs.* Na,[95] there have been several attempts to use different titanate based materials as anodes in sodium ion batteries and specifically $Na_2Ti_3O_7$ has been more deeply studied. On one hand W. Wang *et al.* have predicted by first principle calculations that as many as 3.5 sodium ions per formula unit can be favourably inserted into the $Na_2Ti_3O_7$ structure,[96a] however no more than 2 sodium ions have been reversibly inserted. Additionally, they report that hydrothermally prepared sodium titanate nanotubes with 8 nm outer diameter, when bound with Teflon and carbon black can deliver capacities as high as 108 mA h g^{-1} for 100 cycles at a current density of 350 mA g^{-1} and 85 mA h g^{-1} at rates as high as 3500 mA g^{-1} in 1 M $NaClO_4$ in PC. This implies large power densities, although with quite large coulombic losses for current densities <1700 mA h g^{-1}, which points to side reactions occurring at low current rates, probably associated with the non-optimized electrolyte deployed and the formation of the SEI layer. The same group has reported the preparation of single crystal rods of $Na_2Ti_3O_7$ from sintering at 850 °C the product of synthesis from reverse microemulstion.[96b] The as produced material mixed with MWCNTs (multi walled carbon nanotubes) as conductive additive delivers approximately 180 mA h g^{-1} reversible capacity at C/10 that falls to 103 mA h g^{-1} in 20 cycles. Through the use of NaFSI salt in PC, H. Pan *et al.* have increased the reversible capacity of $Na_2Ti_3O_7$ in the voltage range 0.0–3.0 V (Fig. 29).[97] A deeper study of the electrochemical performance in 1 M $NaClO_4$ EC : PC of the solid state synthesized material has been performed by Rudola *et al.*[98] Although cycling at 5 C reduces the reversible capacity observed at C/10 from 177 mA h g^{-1} to 75 mA h g^{-1}, an improvement in the capacity retention is observed. This is explained by a sodium ion diffusion coefficient as high as 3.48×10^{-12} deduced from impedance measurements at the early stages of discharge, which is higher than that found in the cathode material $Na_4Mn_9O_{12}$. A new oxidation peak has also been reported upon increasing the cutoff voltage from 0.05 to 0.1 V. The origin of this peak is still unknown.

On the side of other different titanates, Xiong *et al.* have used amorphous titanium dioxide nanotubes as anodes.[99] Nanotubes with an inner diameter (id) larger than 80 nm and wall thickness above 15 nm, yield an increasingly large capacity upon cycling in 1 M $NaClO_4$ in PC *vs.* Na metal at C/3, ranging from 60 mA h g^{-1} in the first cycle to 140 mA h g^{-1} after 50 cycles. They have shown that sodium does not intercalate into smaller diameter nanotubes (id < 45 nm)

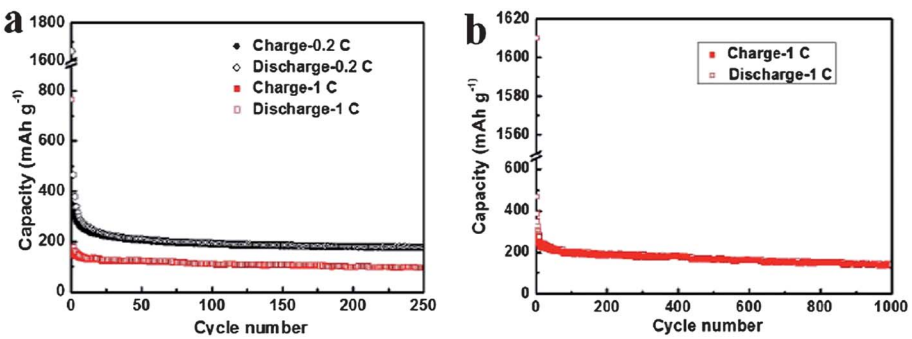

Fig. 28 (a) Cycling performance of RGO at 0.2 C and 1 C for 250 cycles (b) cycling performance of RGO at 1 C for 1000 cycles. Reprinted from Y.-X. Wang, S.-L. Chou, H.-K. Liu and S.-X. Dou, Reduced graphene oxide with superior cycling stability and rate capability for sodium storage, *Carbon*, 2013, **57**, 202–208. Copyright 2013, with permission from Elsevier.

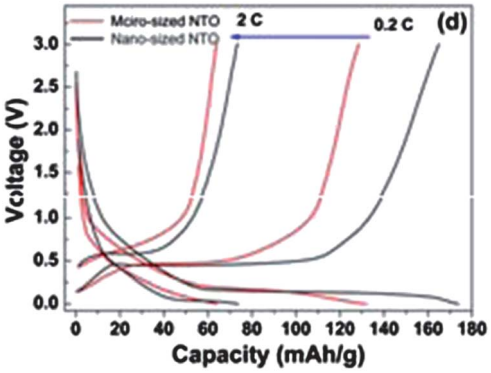

Fig. 29 Discharge/charge curves of the nano- and micro-sized $Na_2Ti_3O_7$ electrodes at different current rates. Reprinted from H. Pan, X. Lu, X. Yu, Y.-S. Hu, H. Li, X.-Q. Yang and L. Chen, Sodium Storage and Transport Properties in Layered $Na_2Ti_3O_7$ for Room-Temperature Sodium-Ion Batteries, *Adv. Energy Mater.*, DOI: 10.1002/aenm.201300139. Copyright 2013, with permission from Wiley.

which they attribute to the solvated sodium ions in the electrolyte not being able to get a critical concentration so as to effectively intercalate into the TiO_2 walls.

The sodium analogue of the zero-strain anode material lithium ion batteries, $Li_4Ti_5O_{12}$, with a spinel structure has not been prepared to date. For the composition $A_4Ti_5O_{12}$ two different sodium based polymorphs are known. A layered like structure closely related to $Na_2Ti_3O_7$ and a 3D tunnel like structure with trigonal symmetry which is the low temperature polymorph. Woo *et al.* have recently studied the electrochemical performance of the low temperature polymorph $Na_4Ti_5O_{12}$ both for lithium and sodium ion batteries.[100] It showed the reversible de/intercalation of Na ions (Fig. 30), but delivered only *ca.* 50 mA h g^{-1}, which is attributed to the poor kinetics of Na ion due to steric hindrance. Nevertheless a thorough study regarding the performance of this material in sodium ion batteries has not been accomplished yet.

Despite a spinel polymorph $Na_4Ti_5O_{12}$ has not been prepared to date, Zhao *et al.* have studied the sodium intercalation into the lithium based spinel $Li_4Ti_5O_{12}$,[101] with a reversible capacity of 145 mA h g^{-1} at about 1.0 V *vs.* Na in $NaClO_4$-PC electrolyte. In this preliminary study *ex situ* XRD data suggest that the final product after three Na insertions might be a mixture of $LiNa_6Ti_5O_{12}$ and $Li_7Ti_5O_{12}$ with a spinel structure and different lattice parameters.

3.2.3 Titanium phosphates. Very recently the low voltage sodium intercalation into the Nasicon type $Na_3Ti_2(PO_4)_3$ based on the Ti(III)/Ti(II) redox pair has opened a new highway for the exploration of titanium based anode materials, which had already been exploited in $LiTiS_2$ materials.[102] As in the case of $Na_2Ti_3O_7$, which inserts at similarly low voltages, capacity fading is a problem that prevents exploitation of this low voltage insertion. However proof of a full titanium based battery is reported.

3.2.4 Carboxylates. One of the most reliable routes to tune the redox potential for sodium insertion has been the use of organic electrodes, based on benzene–carboxylate

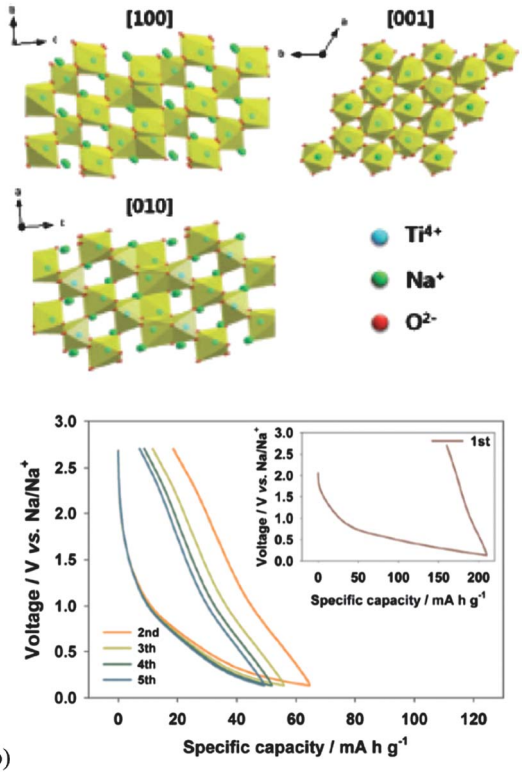

Fig. 30 (a) Crystal structure of trigonal $Na_4Ti_5O_{12}$. (b) Voltage profiles of $Na_4Ti_5O_{12}$ at various cycle number for Na ion batteries. Reproduced by permission of The Electrochemical Society from S. H. Woo, Y. Park, W. Y. Choi, N.-S. Choi,S. Nam, B. Park and K. T. Lee, *J. Electrochem. Soc.*, 2012, **159**, A2016–A2023.

scaffolds chemically modified. Park *et al.* and Zhao *et al.*, evaluated several terephthalate based derivatives and found that disodium terephthalate showed an excellent cyclability with a specific capacity close to 300 mA h g^{-1} over 90 cycles at C/10. The average voltage is 0.4 V *vs.* Na/Na^+, being therefore a promising candidate, which can be produced from low cost renewable sources.[103] For Park's study they used CMC (carboxy methyl cellulose) as a binder and 0.8 M $NaClO_4$ in EC : DEC as electrolyte. Likewise, Abouimrane *et al.*, studied a series of carboxylate materials and found the same disodium terephthalate to have the best performance. In this case, they prepared laminates using sodium alginate as binder and measured with a 1 M $NaPF_6$ in a 3 : 7 EC : EMC mixture electrolyte. After showing that redox sodium insertion happened close to 0.4 V, they used these anodes to assembly full Na-ion based batteries, with Na-layered oxides cathodes, which operated at 3.6 V for more than 50 cycles.[104]

3.2.5 Group 14 and 15 elements – Na alloys. Following the theoretical investigation of sodium alloys with group 14 elements by Chevrier and Ceder in 2011,[105] an increasing activity has flourished about them since they yield the highest capacities. The sodium–tin alloying has been first investigated by Komaba *et al.*[106] in polyacrylate (PAA) based electrodes finding no electrochemical activity in Si or Ge electrodes, and several *plateaux* in Sn of Pb electrodes, with a reversible capacity

of about 500 mA h g^{-1} in Sn electrodes cycled at C/10 for more than 20 cycles. Besides substituting PVdF (polyvinylidene fluoride) binder by PAA, the addition of fluorinated ethylene carbonate (FEC) into the electrolyte[107] has also contributed to the achievement of a good capacity retention. This additive, which so far has not proven valuable when cycling carbon based materials as discussed above, has nonetheless been a key component in all alloy based anodes.

The good cyclability of the tin based electrode has been explained by J. W. Wang *et al.* as due to the absence of particle cracking or fracture, despite a huge volumetric expansion of about 420%.[108] They were able to conclude this by following, using *in situ* electron microscopy, the microstructural evolution of tin nanoparticles during sodium insertion and extraction. Moreover, from the electron diffraction of tin nanoparticles it is possible to deduce that the nanoparticles sodiate first through a two-phase mechanism forming an amorphous sodium poor Na_xSn alloy, which is next sodiated to several sodium rich amorphous phases, (as summarized in Fig. 31) and finally to crystalline $Na_{15}Sn_4$.

Although all studies agree in the composition and crystal structure of the final phase $Na_{15}Sn_5$, Komaba *et al.* assumed that the mechanism of sodiation followed the path predicted by Chevrier *et al.*, whereas a report by Ellis *et al.*,[109] contemporary of that published by Wang *et al.*, proposes the formation of different amorphous intermediates, as observed by *in situ* XRD, with compositions close to $NaSn_3$, NaSn, and Na_9Sn_4. Fig. 32 shows a comparison of their experimental data with the theoretical work by DFT calculations and the OCV measurements taken from the melt.[110]

The electrochemical insertion of sodium into tin has also been studied at intermediate temperatures of 363 K by using a eutectic NaFSA-KFSA (sodium and potassium bis-(fluorosulfonyl)amide) ionic liquid, however capacities lower than 300 mA h g^{-1}, far below those achieved at room temperature, are observed.[111]

On a different approach, Xu *et al.* have produced nanocomposites of porous carbon with tin from dispersions of SnO in a polymer matrix, and they have tested them as anodes for both sodium and lithium ion batteries.[112] Despite the use of an advanced electrode material, its combination with CMC binder and 1 M $NaClO_4$ in EC : DMC (1 : 1) as electrolyte only yields 300 mA h g^{-1} at low current densities which rapidly falls on increasing the C-rate.

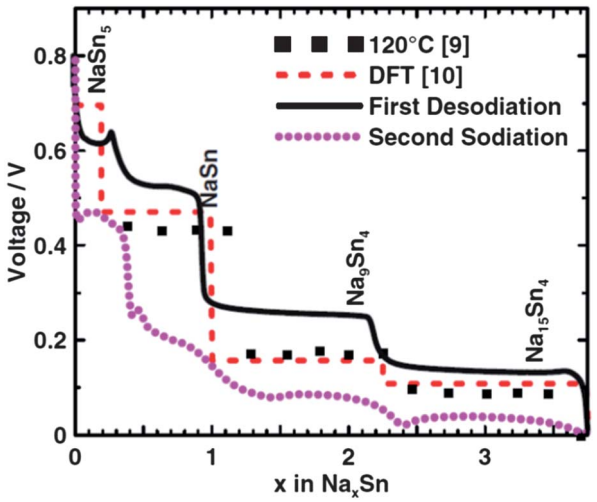

Fig. 32 Voltage curves of the first desodiation and second sodiation of sputtered tin, superimposed on the predicted DFT voltage curve, and open circuit measurements taken at 120 °C by Huggins. Reproduced by permission of The Electrochemical Society from L. D. Ellis, T. D. Hatchard and M. N. Obrovac, *J. Electrochem. Soc.*, 2012, **159**, A1801–A1805.

A similar nanocomposite approach has nonetheless been successful for Sb–C nanocomposites, which in this case use metallic powder as starting material. The mechanically mixed nanocomposite offers a high capacity of 610 mA h g^{-1} (corresponding to the storage of 3 Na ions) for more than 100 cycles at C/6 when a 5% FEC is added to a 1 M $NaPF_6$ EC : DEC (1 : 1) electrolyte, showing to be a feasible alternative alloying material.[113] Moreover, capacities as large as 300 mA h g^{-1} are achieved at high rates of 2000 mA g^{-1}. Despite this anode is capable of giving a reversible capacity as large as those of tin based electrodes, the average voltage is higher and therefore the energy density of the final full battery will be reduced with respect to that of a battery deploying a tin based anode.

More strikingly, commercial micrometric Sb has also proven to have reversible specific capacities of 600 mA h g^{-1}, close to the theoretical one, maintained over 150 cycles with a coulombic efficiency of 98%, which turns out to outperform the numbers for the same material in a lithium ion battery.[114] A comparison of the performance of bulk Sb in lithium and sodium is given in Fig. 33. The addition of a 5% FEC additive in the electrolyte, while being a key component for the stability of

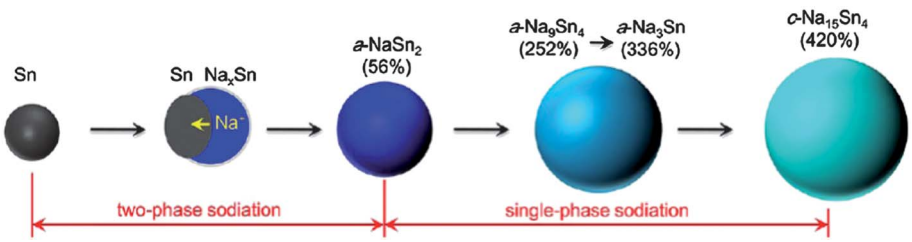

Fig. 31 Schematic illustration of the structural evolution of Sn NPs during the sodiation. Reprinted with permission from J. W. Wang, X. H. Liu, S. X. Mao and J. Y. Huang, *Nano Lett.*, 2012, **12**, 5897–5902. Copyright 2012 American Chemical Society.

the SEI layer in the sodium ion electrode, does not explain in itself the better cyclability of the sodium *vs.* lithium electrode. *In situ* XRD during the electrochemical testing showed that the absence of crystalline Na_xSb intermediate phases between Sb and Na_3Sb end members could be the reason for its better performance.

SnSb alloys prepared by high energy ball milling have also been evaluated as anodes in composites with CMC binder *vs.* sodium in 1 M $NaClO_4$ in EC : DMC electrolyte.[115] While XRD diffraction shows that a single phase SnSb alloy forms, the redox peaks found in the CV measurements suggests that Sn rich and Sb rich phases react sequentially, in a similar fashion to the reaction with lithium, although to date it has not been confirmed by diffraction techniques. A capacity as high as 500 mA h g^{-1} is delivered at C/5 with an 80% capacity retention after 50 cycles, which are reasonably good values considering the huge volumetric expansions that sodium based alloys suffer upon cycling.

Based on the same alloying reaction of Sn, and likely preceded by the conversion of SnO_2 into Sn + Na_2O, a composite electrode of SnO_2 and graphene has reported the capacities, above 600 mA h g^{-1} at 40 mA g^{-1}.[116] In this composite as much as 40% weight is carbon, however, as in the case of many other composite electrodes the capacity refers only to the weight of active material. SnO_2 octahedra, 60 nm in edge, embedded in graphene are produced in a single hydrothermal step that delivers 300 mA h g^{-1} at rates of 160 mA g^{-1} in 1 M $NaClO_4$ EC : PC. While the capacity is as large as that of Sb–C composites, the power is lower and the voltage range for delivering this capacity is larger, between 0 and 3 V.

3.2.6 Binary compounds reacting through conversion reactions. Sun *et al.* showed that a reversible capacity as large as 800 mA h g^{-1} could be achieved for SbO_2 undergoing conversion followed by alloying reactions at C/70 in 1 M $NaClO_4$ in EC : DMC.[117] A voltage hysteresis larger than 1 V as in the case of lithium-ion batteries was observed. A recent work by Balaya *et al.* reported 350 mA h g^{-1} at 0.06 C for Fe_3O_4–C nanocomposites as electrode materials for sodium ion batteries, and 950 mA h g^{-1} for lithium ones.[118] The team worked on improving the adhesion of the material to the current collector by heat treating the electrode at 250 C for 3 h, which significantly improved the capacity retention. The material was tested *vs.* sodium in the 0–3 V range in a standard 1 M $NaClO_4$ EC : PC electrolyte with 70% charge capacity retention after 10 cycles. Selected area electron diffraction patterns of cycled electrodes prove the formation of the conversion products Fe and Na_2O as well as the coexistence of Fe_3O_4 with remaining Fe and Na_2O upon charge.

Thin films of Fe_2O_3–NiO solid solutions prepared by Lopez *et al.* by electrodeposition and subsequent thermal treatment showed an improved reversibility in the 0–3.0 V voltage range with respect to the same films of the end members, showing the synergistic effect that solid solutions have on the electrochemical performance of conversion materials.[119]

As in the case of lithium-ion batteries, conversion reactions offer an attractive range of large theoretical specific capacities. However, besides the always present voltage hysteresis, these values are achieved over quite large voltage ranges (Table 3). Alloying and intercalation materials, on the other hand, deliver their charge in more limited potential ranges which enables higher voltage full cells.

3.2.7 Amorphous phosphorous. The latest development in the field of anode materials has been made simultaneously in two Korean laboratories by the use of ball milled red phosphorus with conductive carbon until an amorphous mixture is obtained. Qian *et al.* have obtained a reversible capacity in excess of 1500 mA h g^{-1} of phosphorus at a rate of 250 mA g^{-1} that with the use of FEC additive remains 1100 mA h g^{-1} after 100 cycles.[120] A more stable reversible capacity of 1890 mA h g^{-1} is measured in the phosphorus–carbon composites studied by Y. Kim *et al.* which were prepared with PAA binder.[121] In this work, *ex situ* XRD data show the formation of Na_3P at the end of discharge.

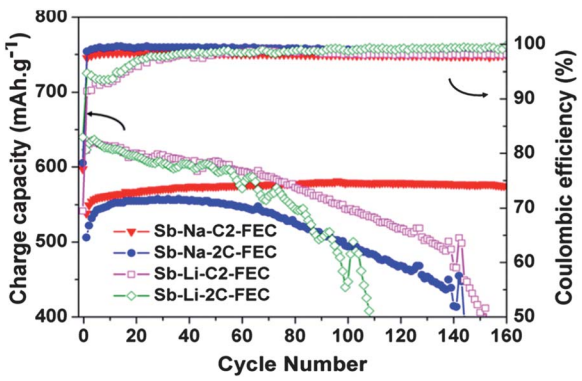

Fig. 33 Cycling performance of Sb electrode *vs.* Na^+ and Li^+ at C/2 and 2 C with 5% FEC additive. Reprinted with permission from A. Darwiche, C. Marino, M. T. Sougrati, B. Fraisse, L. Stievano and L. Monconduit, *J. Am. Chem. Soc.*, 2012, **134**, 20805–20811. Copyright 2012 American Chemical Society.

4 $Na–O_2$ batteries

As has previously been commented, more than a decade of research into energy storage platforms has helped define the magnitude of the challenges that must be overcome for batteries to catch up with present and future needs of society. One of them is the achievement of higher specific energy in order to satisfy the demand of power supply in the vehicle industry or portable electronic technology, for example. For this reason, much effort has been devoted to develop rechargeable metal–oxygen batteries in the last years, namely, Zn–air[122–124] and Li–air[125–128] technologies.

Metal–oxygen batteries consist of a porous air electrode where oxygen reacts with alkali metal ions to produce the corresponding alkali oxides. It must be remarked that, although these systems are mainly called "metal–air" they are "metal–oxygen batteries", because it is only oxygen which reacts electrochemically and water, CO_2 and other air components must be removed previously in order to achieve reversibility of the system.

Table 3 Summary of most relevant theoretical and largest experimentally observed reversible capacities in anode systems for sodium-ion batteries[a]

Compound	Theoretical Csp (mA h g^{-1})	Experimental. reversible Csp (mA h g^{-1})	Voltage range (V)	Reference
Hard carbon	—	350	~0 to 1.0 V	88
$Na_4Ti_5O_{12}$	(1Na)	60		109
$Li_4Ti_5O_{12}$	(3 Na)	145	0.8 V	101
$Na_2Ti_3O_7$	177 (2Na)	177	~0.3 V	95
$Na_3Ti_2(PO_4)_3$	130–140 (2Na)	130–140	2.0 V	17 and 102
NaHBDC-carboxylate	270(2–4Na)	270	~0.3 V	103 and 104
Sn	850 (4.4Na)	850	0.2–1.0 V	106
Sb	660 (3Na)	580	0.04–1.5 V	113
SnO_2/graphene	1378 (8.4Na)	600	0–3.0 V	116
Fe_3O_4	926 (8Na)	~350	0.04–3.0 V	118
P	2596 (3Na)	~1764	0–2.0 V	120 and 121

[a] Exp: experimental.

The porous electrode, which is usually made of porous carbon and/or porous metal, has two functions. The first is to act as a current delivery system for the reduction of O_2, and the second is to host the product of this reaction by filling the voids and pores in its structure. For this purpose, a catalyst dispersed on the porous matrix is often needed. Fig. 34 shows the scheme of a metal–O_2 battery.[129]

The use of sodium as alkali metal in this kind of batteries can be beneficial for several reasons:

- First, its adequate electrode potential and specific energy (1600 W h kg^{-1} based on $2Na^+ + O_2 + 2e^- \rightarrow Na_2O_2$ reaction at 2.33 V).[130]
- Second, the feasibility of forming the stable superoxide NaO_2 apart from Na_2O, a condition that Li does not fulfil.
- Third, the known arguments about its natural abundance and low cost.

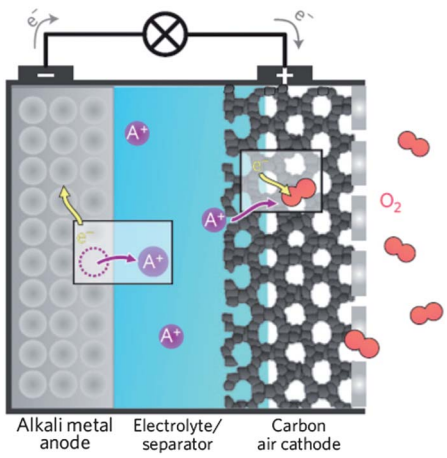

Fig. 34 Scheme of a metal–O_2 battery. During discharge, metal A is oxidized to a soluble A^+ cation at the anode–electrolyte interface and the electron is transferred to the outer circuit. At the cathode side, O_2 is reduced to a superoxide or oxide species that may form an alkali superoxide or oxide in the presence of A^+ cations. Charge is based on the reversibility of this process. Reprinted by permission from Macmillan Publishers Ltd: P. Hartmann, C. L. Bender, M. Vračar, A. K. Dürr, A. Garsuch, J. Janek and P. Adelhelm, *Nat. Mater.*, 2013, **12**, 228–232. Copyright 2013.

Although up until now there haven't been many references about this kind of batteries, very different approaches have been used up to focus the research. The cell configuration for all these systems is summarised in Table 4.

Peled *et al.* proposed the use of liquid sodium as anode by operating the Na–O_2 cell above the sodium melting point (97.8 °C).[131] The advantages of this kind of system would be the following: (i) elimination of the possibility of dendrite formation, (ii) the high operating temperature, which favours electrode kinetics acceleration, can reduce cell internal resistance and minimizes the water vapour in the system, (iii) the feasibility of using Al as light and low-cost hardware material (as Na does not dissolve into Al), and (iv) the fact that Na does not form a nitride in air, as Li does, that could lead to parasitic reactions. The system proposed by these authors demonstrated the feasibility of an intermediate temperature operating Na–O_2 cell. A recent publication goes deeper into the understanding of the processes in both the sodium and porous electrodes.[132]

Sun *et al.* were the first to demonstrate that a room temperature sodium–O_2 cell could work.[133] They prepared a non-aqueous Na–O_2 cell based on a diamond-like carbon thin film (DLC). They got up to a 2070 mA h g^{-1} discharge capacity value in the third cycle that declined to 1058 mA h g^{-1} in the 20th cycle (Fig. 35), and the rate capability showed that discharge capacities diminished from 3600 mA h g^{-1} at C/60 to 180 mA h g^{-1} at 3 C. Thus, this cell needs to be improved both in cycle life and rate performance. They also observed that carbonate solvents in the electrolyte decomposed when discharging below 1.5 V.

A recent work by Hartmann *et al.* reports on a sodium–O_2 cell that can reversibly operate with very low overpotentials (<200 mV) and relatively high current densities (0.2 mA cm^{-2}) by using a pure carbon cathode without catalyst.[129] This system presents the advantage of using a free-standing, binder-free GDL with a low surface area electrode that excludes unwanted reactions due to binder decomposition, minimizes unknown influences from the carbon surface chemistry, and allows the accommodation of reaction products in its macroporous network. This work demonstrates that cell reaction takes place in the whole cathode volume and verifies that NaO_2 is the main

Table 4 Cell configuration for the different proposed systems for Na–O_2 batteries

System	Anode	Electrolyte	Cathode	OCV	Charge/discharge profile	Ref.
High temperature cell	Molten Na	CP[a] anion trap, 1 M $NaClO_4$, 1% w/w Al_2O_3 in PEGDME[b]–propylene carbonate (90 : 10)	E-TEK electrode coated with Al_2O_3.	~2V	Charge: 3 V Discharge: 1.75 V 85% Faradaic efficiency	131
Room temperature cell	Metallic Na	1 M $NaPF_6$ in EC:PC (1:1)	Diamond Like Carbon (DLC)	2.98 V	Charge: < 3.5 V Discharge: 2.36–2.0 V (2 pseudo*plateaux*)	133
Room temperature cell	Metallic Na	0.5 M $NaSO_3CF_3$ in DEGDME[c] supported on glass fibre	GDL (carbon-fibre gas diffusion layer)	—	Charge: 2.3–2.4 V Discharge: 2.2 V	129
CO_2 assisted Na–O_2 cell	Metallic Na	1 M $NaClO_4$ in TEGDME[d] or 0.75 M $NaSO_3CF_3$ in ENIM Otf[e]	90% Super P (TIMCAL) carbon 10% PVdF	—	Discharge: ~2.3 V	130
Room temperature cell	Metallic Na	$NaClO_4$ or $NaPF_6$ in DME	Graphene nanosheets	~3 V	Charge: 4 V Discharge: ~2.8 V	134

[a] Calyx[6]pyrrole. [b] Polyethyleneglycol dimethyl ether. [c] Diethylene glycol dimethyl ether. [d] Tetraethylene glycol dimethyl ether. [e] 1-Ethyl-3-methyl imidazolium trifluoromethanesulfonate.

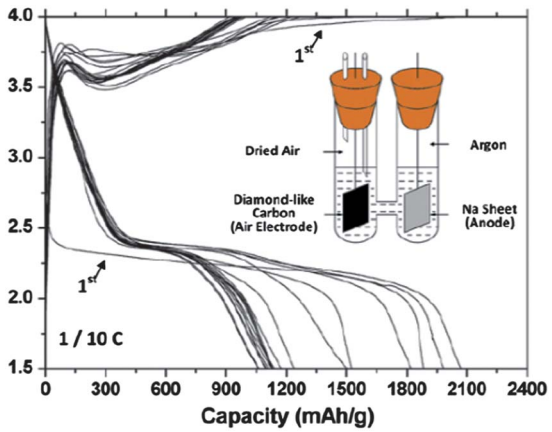

Fig. 35 Galvanostatic cycling profiles of the DLC thin film-based cell. Inset: scheme and composition of the cell. Reprinted from Q. Sun, Y. Yang and Z.-W. Fu, Electrochemical properties of room temperature sodium–air batteries with non-aqueous electrolyte, *Electrochem. Commun.*, 2012, **16**, 22–25. Copyright 2012, with permission from Elsevier.

reaction product. This compound demonstrated to be stable and showed no degradation in discharged cathodes or during *ex situ* analysis. Fig. 36 shows the proposed reactions taking place in the cathode.

Graphene nanosheets (GN) have also been used as cathodes in a Na–O_2 cell with excellent results by Liu *et al.*[134] They demonstrate that the Na/GN system presents lower over-potential and higher operating potential than a thin film carbon electrode. Moreover, graphene nanosheets work under larger currents and present highs specific capacities at different rates. This cell displays a discharge capacity of 9268 mA h g^{-1} and 1110 at a 200 and 1000 mA g^{-1} current, respectively. GN electrode offers these good electrochemical features due to its high porosity and large surface area (83 m^2 g^{-1}), and its high electron mobility, with an electrical conductivity of 68 S cm^{-1}. This way, the material possesses more active sites for the cathode reaction to occur and presents enhanced electron transportation to/from the active sites during the electrochemical reaction.

Das *et al.* have developed a novel approach to sodium–O_2 cells, evaluating them not only as an energy conversion device but also as a platform for capturing CO_2 from a CO_2-rich gas stream.[130] They have demonstrated that the specific energy of a Na–O_2 cell can be enhanced by factors of 2 or 3 by introducing optimized concentrations of CO_2 (Fig. 37). This gas is captured by producing Na_2CO_3 and/or $Na_2C_2O_4$ in the cathode depending on the electrolyte used. For this reason, this kind of batteries would not be considered as secondary rechargeable systems, but as primary ones, because accumulation of sodium carbonate and oxalate in the cathode would finally block the electrode reaction.

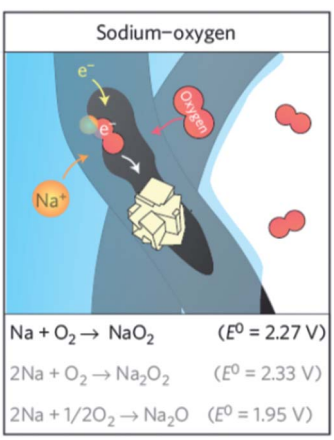

Fig. 36 In black, the main reaction taking place in the cathode. In grey, other possible cell reactions that have not been observed experimentally. Reprinted by permission from Macmillan Publishers Ltd: P. Hartmann, C. L. Bender, M. Vračar, A. K. Dürr, A. Garsuch, J. Janek and P. Adelhelm, *Nat. Mater.*, 2013, **12**, 228–232. Copyright 2013.

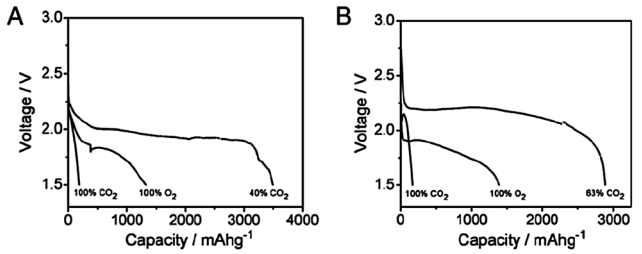

Fig. 37 Galvanostatic discharge profiles for Na–CO_2/O_2 cells operated with different O_2/CO_2 feeds by using (a) 0.75 M NaTFSI in ENIM Otf ionic liquid electrolyte, and (b) 1 M $NaClO_4$ in TEGDME tetraglyme electrolyte. Reprinted from S. K. Das, S. Xu and L. A. Archer, Carbon dioxide assist for non-aqueous sodium–oxygen batteries, *Electrochem. Commun.*, 2013, **27**, 59–62. Copyright 2013, with permission from Elsevier.

5 Conclusions

As has been shown, research on Na-based energy storage systems is continuously growing in order to face the very different challenges of each of the mentioned battery chemistries that are summarized below.

Concerning the aqueous systems, they hold promise for their low cost, especially when applied to stationary applications. Many other materials that meet the target in terms of performance and cycle life while keeping the cost extremely low can still be found.

With respect to Na-ion non-aqueous battery cathodes, several compounds must be taken into account. The potential of layered oxide materials as a high capacity Na-ion battery cathodes is quite bright due to the many factors mentioned already, but there is much to learn about this system before this material can be used in a real battery. On the other hand, phosphates and fluorophosphates present an excellent stability and a great variety of operating voltages. In spite of the long way off to commercial Na-ion batteries, these features place them closer to the real market.

Regarding the anode materials for these systems, much progress has been made in hardly one year, achieving quite large specific capacities in alloy based materials. However, for a cost effective, large scale application system the hope is to find or develop better carbon based or titanium oxide or polyanionic based systems capable of reversibly inserting sodium at quite low voltages with stable SEI layer formation.

With respect to Na-oxygen systems, they can be the key technology to overcome the need for high energy density storage devices, but much work is needed in this field to demonstrate which is the most viable Na–O_2 chemistry (based on Na_2O_2 or NaO_2) and to develop it. New focuses on this technology, like the one that combines CO_2 capture with energy conversion, open fresh and valuable research lines.

Acknowledgements

This work was financially supported by the Ministerio de Educación y Ciencia (MAT2010-19442) and the Gobierno Vasco/EuskoJaurlaritza (EtortekCICEnergigune 10, SAIOTEK-12 ENERGIBA and IT570-13).

References

1 B. L. Ellis and L. F. Nazar, *Curr. Opin. Solid State Mater. Sci.*, 2012, **16**, 168–177.
2 K. B. Hueso, M. Armand and T. Rojo, *Energy Environ. Sci.*, 2013, **6**, 734–749.
3 V. Palomares, P. Serras, I. Villaluenga, K. B. Hueso, J. Carretero-González and T. Rojo, *Energy Environ. Sci.*, 2012, **5**, 5884–5901.
4 I. Villaluenga, M. Armand and T. Rojo, Hybrid Electrolytes,2012, PCT/EP2013/051023.
5 J. W. Fergus, *Solid State Ionics*, 2012, **227**, 102–112; I. Villaluenga, X. Bogle, S. Greenbaum, I. Gil de Muro, T. Rojo and M. Armand, *J. Mater. Chem. A*, 2013, **1**(29), 8348–8352.
6 F. Sauvage, E. Baudrin and J. M. Tarascon, *Sens. Actuators, B*, 2007, **120**(2), 638–644.
7 J. F. Whitacre, A. Tevar and S. Sharma, *Electrochem. Commun.*, 2010, **12**(3), 463–466.
8 Whitacre, *US Pat.* no. 2009/0253025 A1, 2009.
9 Whitacre, *US Pat.* no. 2011/0052945 A1, 2011.
10 Whitacre, *US Pat.* no. 2011/0274950 A1, 2011.
11 J. F. Whitacre, T. Wiley, S. Shanbhag, Y. Wenzhuo, A. Mohamed, S. E. Chun, E. Weber, D. Blackwood, E. Lynch-Bell, J. Gulakowski, C. Smith and D. Humphreys, *J. Power Sources*, 2012, **213**, 255–264.
12 http://www.aquionenergy.com/.
13 C. D. Wessells, R. A. Huggins and Y. Cui, *Nat. Commun.*, 2011, **2**, 550.
14 C. D. Wessells, S. V. Peddada, R. A. Huggins and Y. Cui, *Nano Lett.*, 2011, **11**, 5421–5425.
15 M. D. Levi, S. Sigalov, G. Salitra, R. Elazari, D. Aurbach, L. Daikhin and V. Presser, *J. Phys. Chem. C*, 2013, **117**, 1247–1256.
16 S. I. Park, I. Gocheva, S. Okada and J. Yamaki, *J. Electrochem. Soc.*, 2011, **158**, A1067–A1070.
17 Z. Li, D. Young, K. Xiang, W. C. Carter and Y. M. Chiang, *Adv. Energy Mater.*, 2013, **3**, 290–294.
18 N. Yabuuchi, M. Kajiyama, J. Iwatate, H. Nishikawa, S. Hitomi, R. Okuyama, R. Usui, Y. Yamada and S. Komaba, *Nat. Mater.*, 2012, **11**, 512–517.
19 R. Fielden and M. N. Obrovac, Structure and electrochemistry of $NaNiO_2$, poster at: Honolulu PRiME 2012, 2012 Fall Meeting of The Electrochemical Society, Honolulu, Hi, 2012 Oct. 7 – 12.
20 P. Vassilaras, X. Ma, X. Lin and G. Ceder, *J. Electrochem. Soc.*, 2012, **160**, A207–A211.
21 H. Yoshida, N. Yabuuchi and S. Komaba, Na insertion mechanism in α-$NaFeO_2$ as positive electrode materials for Na-ion batteries, paper presented at: Honolulu PRiME 2012, 2012 Fall Meeting of The Electrochemical Society, Honolulu, Hi, 2012 Oct. 7–12.
22 C. Y. Chen, K. Matsumoto, T. Nohira, R. Hagiwara, K. Numata, E. Itani, A. Fukunaga, S. Sakai, K. Nitta and S. Inazawa, Structural investigation of $NaCrO_2$ as a positive electrode for rechargeable sodium battery using molten NaFSA-KFSA, paper presented at: HonoluluPRiME

2012, 2012 Fall Meeting of The Electrochemical Society, Honolulu, Hi, 2012 Oct. 7–12.
23 J. J. Ding, Y. N. Zhou, Q. Sun and Z. W. Fu, *Electrochem. Commun.*, 2012, **22**, 85–88.
24 S. Komaba, C. Takei, T. Nakayama, A. Ogata and N. Yabuuchi, *Electrochem. Commun.*, 2010, **12**, 355.
25 S. K. Hu, G. H. Cheng, M. Y. Cheng, B. J. Hwang and R. Santhanam, *J. Power Sources*, 2009, **188**, 564–569.
26 Y. Q. Wang, Z. P. Liu and S. M. Zhou, *Electrochim. Acta*, 2011, **58**, 359–363.
27 M. D'Arienzo, R. Ruffo, R. Scotti, F. Morazzoni, C. M. Mari and S. Polizzi, *Phys. Chem. Chem. Phys.*, 2012, **14**, 5945–5952.
28 J. J. Ding, Y. N. Zhou, Q. Sun, X. Q. Yu, X. Q. Yang and Z. W. Fu, *Electrochim. Acta*, 2013, **87**, 388–393.
29 D. H. Lee, J. Xu and Y. S. Meng, Na-ion intercalation cathode with high rate and excellent structural stability, paper presented at: Honolulu PRiME 2012, 2012 Fall Meeting of The Electrochemical Society, Honolulu, Hi, 2012 Oct. 7–12.
30 S. Komaba, N. Yabuuchi, T. Nakayama, A. Ogata, T. Ishikawa and I. Nakai, *Inorg. Chem.*, 2012, **51**, 6211–6220.
31 J. S. Thorne, R. A. Dunlap and M. N. Obrovac, Structure and electrochemistry of $Na_xFe_xMn_{1-x}O_2$ Na-ion cathode materials, paper presented at: Honolulu PRiME 2012, 2012 Fall Meeting of The Electrochemical Society, Honolulu, Hi, 2012 Oct. 7–12.
32 D. Kim, E. Lee, M. Slater, W. Lu, S. Rood and C. S. Johnson, *Electrochem. Commun.*, 2012, **18**, 66–69.
33 M. Sathiya, K. Hemalatha, K. Ramesha, J.-M. Tarascon and A. S. Prakash, *Chem. Mater.*, 2012, **24**, 1846–1853.
34 C. Didier, M. Guignard, J. Darriet and C. Delmas, *Inorg. Chem.*, 2012, **51**, 11007–11016.
35 D. Yuan, W. He, F. Pei, F. Wu, Y. Wu, J. Qian, Y. Cao, X. Ai and H. Yang, *J. Mater. Chem. A*, 2013, **1**, 3895–3899.
36 J. M. Paulsen and J. R. Dahn, *Solid State Ionics*, 1999, **126**, 3–24.
37 D. Buchholz, A. Moretti, R. Kloepsch, S. Nowak, V. Siozios, M. Winter and S. Passerini, *Chem. Mater.*, 2013, **25**, 142–148.
38 X. Xia and J. R. Dahn, A study of the reactivity of de-intercalated $NaNi_{0.5}Mn_{0.5}O_2$ with non-aqueous solvent and electrolyte by accelerating rate calorimetry, paper presented at: Honolulu PRiME 2012, 2012 Fall Meeting of The Electrochemical Society, Honolulu, Hi, 2012 Oct. 7–12.
39 X. Xia and J. R. Dahn, *J. Electrochem. Soc.*, 2012, **159**, A647–A650.
40 S. Tepavcevic, H. Xiong, V. R. Stamenkovic, X. Zuo, M. Balasubramanian, V. B. Prakapenka, C. S. Johnson and T. Rajh, *ACS Nano*, 2012, **6**, 530–538.
41 B. Koo, S. Chattopadhyay, T. Shibata, V. B. Prakapenka, C. S. Johnson, T. Rajh and E. V. Shevchenko, *Chem. Mater.*, 2013, **25**, 245–252.
42 Y. H. Jung, S. T. Hong and D. K. Kim, Electrochemical sodium ion intercalation property of $Na_{2.7}Ru_4O_9$ in nonaqueous and aqueous electrolytes, paper presented at: Honolulu PRiME 2012, 2012 Fall Meeting of The Electrochemical Society, Honolulu, Hi, 2012 Oct. 7–12.
43 S. M. Oh, S. T. Myung, J. Hassoun, B. Scrosati and Y. K. Sun, *Electrochem. Commun.*, 2012, **22**, 149–152.
44 M. Casas-Cabanas, V. V. Roddatis, D. Saurel, P. Kubiak, J. Carretero-González, V. Palomares, P. Serras and T. Rojo, *J. Mater. Chem.*, 2012, **22**(34), 17421–17423.
45 Y. Zhu, Y. Xu, Y. Liu, C. Luo and C. Wang, *Nanoscale*, 2013, **5**, 780–787.
46 Y. Liu, Y. Xu, X. Han, C. Pellegrinelli, Y. Zhu, H. Zhu, J. Wan, A. Chong Chung, O. Vaaland, C. Wang and L. Hu, *Nano Lett.*, 2012, **12**, 5664–5668.
47 C. Delmas, R. Olazcuaga, F. Cherkaoui and R. Brochu, *C.R. Acad. Sc. Paris, Ser. C*, 1978, **287**, 169–171.
48 J. Gopalakrishnan and K. K. Rangan, *Chem. Mater.*, 1992, **4**, 745–747.
49 B. L. Cushing and J. B. Goodenough, *J. Solid State Chem.*, 2001, **162**, 176–181.
50 S. Y. Lim, H. Kim, R. A. Shakoor, Y. Jung and J. W. Choi, *J. Electrochem. Soc.*, 2012, **159**, A1393–A1397.
51 Z. Jian, L. Zhao, H. Pan, Y.-S. Hu, H. Li, W. Chen and L. Chen, *Electrochem. Commun.*, 2012, **14**, 86–89.
52 Z. Jian, W. Han, X. Lu, H. Yang, Y.-S. Hu, J. Zhou, Z. Zhou, J. Li, W. Chen, D. Chen and L. Chen, *Adv. Energy Mater.*, 2013, **3**, 156–160.
53 J. Kang, S. Baek, V. Mathew, J. Gim, J. Song, H. Park, E. Chae, A. K. Rai and J. Kim, *J. Mater. Chem.*, 2012, **22**, 20857–20860.
54 M. Pivko, I. Arcon, M. Bele, R. Dominko and M. Gaberscek, *J. Power Sources*, 2012, **216**, 145–151.
55 L. S. Plashnitsa, E. Kobayashi, Y. Noguchi, S. Okada and J. Yamaki, *J. Electrochem. Soc.*, 2010, **157**, A536–A543.
56 Y. Noguchi, E. Kobayashi, L. S. Plashnitsa, S. Okada and J.-I. Yamaki, *Electrochim. Acta*, 2013, **101**, 59–65.
57 K. Chihara, A. Kitajou, I. D. Gocheva, S. Okada and J.-I. Yamaki, *J. Power Sources*, 2013, **227**, 80–85.
58 R. A. Shakoor, D.-H. Seo, H. Kim, Y.-U. Park, J. Kim, S.-W. Kim, H. Gwon, S. Lee and K. Kang, *J. Mater. Chem.*, 2012, **22**, 20535–20541.
59 J.-M. Le Meins, M.-P. Crosnier-Lopez, A. Hemon-Ribaud and G. Courbion, *J. Solid State Chem.*, 1999, **148**, 260–277.
60 F. Sauvage, E. Quarez, J. Tarascon and E. Baudrin, *Solid State Sci.*, 2006, **8**, 1215–1221.
61 P. Serras, V. Palomares, A. Goñi, I. Gil de Muro, P. Kubiak, L. Lezama and T. Rojo, *J. Mater. Chem.*, 2012, **22**, 22301–22308.
62 P. Serras, V. Palomares, A. Goñi, P. Kubiak and T. Rojo, *J. Power Sources*, 2013, **241**, 56–60.
63 B. L. Ellis, W. R. M. Makahnouk, W. N. Rowan-Weetaluktuk, D. H. Ryan and L. F. Nazar, *Chem. Mater.*, 2010, **22**, 1059–1070.
64 O. V. Yakubovich, O. V. Karimova and O. K. Mel'nikov, *Acta Crystallogr., Sect. C: Cryst. Struct. Commun.*, 1997, **53**, 395–397.
65 N. Recham, J. N. Chotard, L. Dupont, K. Djellab, M. Armand and J. M. Tarascon, *J. Electrochem. Soc.*, 2009, **156**, A993–A999.
66 Y. Kawabe, N. Yabuuchi, M. Kajuyama, N. Fukuhara, T. Inamasu, R. Okuyama, I. Nakai and S. Komaba, *Electrochem. Commun.*, 2011, **13**, 1225–1228.

67 A. Langrock, Y. Xu, Y. Liu, S. Ehrman, A. Manivannan and C. Wang, *J. Power Sources*, 2013, **223**, 62–67.
68 X. Wu, J. Zheng, Z. Gong and Y. Yang, *J. Mater. Chem.*, 2011, **21**, 18630–18637.
69 Y. Kawabe, N. Yabuuchi, M. Kajiyama, N. Fukuhara, T. Inamasu, R. Okuyama, I. Nakai and S. Komaba, *Electrochemistry*, 2012, **80**, 80–84.
70 S.-W. Kim, D.-H. Seo, H. Kim, K.-Y. Park and K. Kang, *Phys. Chem. Chem. Phys.*, 2012, **14**, 3299–3303.
71 P. Barpanda, S.-I. Nishimura and A. Yamada, *Adv. Energy Mater.*, 2012, **2**, 841–859.
72 P. Barpanda, M. Avdeev, C. D. Ling, J. Lu and A. Yamada, *Inorg. Chem.*, 2013, **52**, 395–401.
73 P. Barpanda, T. Ye, S.-I. Nishimura, S.-C. Chung, Y. Yamada, M. Okubo, H. Zhou and A. Yamada, *Electrochem. Commun.*, 2012, **24**, 116–119.
74 H. Kin, R. A. Shakoor, C. Park, S. Y. Lim, J.-S. Kim, Y. N. Jo, W. Cho, K. Miyasaka, R. Kahraman, Y. Jung and J. W. Choi, *Adv. Funct. Mater.*, 2013, **23**, 1147–1155.
75 T. Honma, N. Ito, T. Togashi, A. Sato and T. Komatsu, *J. Power Sources*, 2013, **227**, 31–34.
76 H. Kim, I. Park, D.-H. Seo, S. Lee, S.-W. Kim, W. J. Kwon, Y.-U. Park, C. S. Kim, S. Jeon and K. Kang, *J. Am. Chem. Soc.*, 2012, **134**, 10369–10372.
77 C. S. Park, H. Kim, R. A. Shakoor, E. Yang, S. Y. Lim, R. Kahraman, Y. Jung and J. W. Choi, *J. Am. Chem. Soc.*, 2013, **135**, 2787–2792.
78 M. Tamaru, P. Barpanda, Y. Yamada, S.-I. Nishimura and A. Yamada, *J. Mater. Chem.*, 2012, **22**, 24526–24529.
79 N. Furuta, S.-I. Nishimura, P. Barpanda and A. Yamada, *Chem. Mater.*, 2012, **24**, 1055–1061.
80 S. P. Ong, V. L. Chevrier and G. Ceder, *Phys. Rev. B: Condens. Matter Mater. Phys.*, 2011, **83**, 075112.
81 Y. Lu, L. Wang, J. Cheng and J. B. Goodenough, *Chem. Commun.*, 2012, **48**, 6544–6546.
82 L. Wang, Y. Lu, J. Liu, M. Xu, J. Cheng, D. Zhang and J. B. Goodenough, *Angew. Chem., Int. Ed.*, 2013, **52**, 1964–1967.
83 R. Zhao, L. Zhu, Y. Cao, X. Ai and H. X. Yang, *Electrochem. Commun.*, 2012, **21**, 36–38.
84 M. Zhou, Y. Xiong, Y. Cao, X. Ai and H. Yang, *J. Polym. Sci., Part B: Polym. Phys.*, 2013, **51**, 114–118.
85 N. Recham, G. Rousse, M. T. Sougrati, J.-N. Chotard, C. Frayret, S. Mariyappan, B. C. Melot, J.-C. Jumas and J.-M. Tarascon, *Chem. Mater.*, 2012, **24**, 4363–4370.
86 S. Wenzel, T. Hara, J. Janek and P. Adelhelm, *Energy Environ. Sci.*, 2011, **4**, 3342–3345.
87 S. Komaba, W. Murata, T. Ishikawa, N. Yabuuchi, T. Ozeki, T. Nakayama, A. Ogata, K. Gotoh and K. Fujiwara, *Adv. Funct. Mater.*, 2011, **21**, 3859–3867.
88 A. Ponrouch, E. Marchante, M. Courty, J. M. Tarascon and M. R. Palacin, *Energy Environ. Sci.*, 2012, **5**, 8572–8583.
89 A. Ponrouch, A. R. Goñi and M. R. Palacin, *Electrochem. Commun.*, 2013, **27**, 85–88.
90 Y. Cao, L. Xiao, M. L. Sushko, W. Wang, B. Schwenzer, J. Xiao, Z. Nie, L. V. Saraf, Z. Yang and J. Liu, *Nano Lett.*, 2012, **12**, 3783–3787.
91 K. Tang, L. Fu, R. J. White, L. Yu, M. M. Titirici, M. Antonietti and J. Maier, *Adv. Energy Mater.*, 2012, **2**, 873.
92 Y.-X. Wang, S.-L. Chou, H.-K. Liu and S.-X. Dou, *Carbon*, 2013, **57**, 202–208.
93 Z. Wang, L. Qie, L. Yuan, W. Zhang, X. Hu and Y. Huang, *Carbon*, 2013, **55**, 328–334.
94 H. Wang, Z. Wu, F. Meng, D. Ma, X. Huang, L. Wang and X. Zhang, *ChemSusChem*, 2013, **6**, 56–60.
95 P. Senguttuvan, G. Rousse, V. Seznec, J. M. Tarascon and M. R. Palacín, *Chem. Mater.*, 2011, **23**, 4109–4111.
96 (*a*) W. Wang, C. Yu, Z. Lin, J. Hou, H. Zhua and S. Jiao, *Nanoscale*, 2013, **5**, 594–599; (*b*) W. Wang, C. Yu, Z. Lin, J. Hou, H. Zhua and S. Jiao, *RSC Adv.*, 2013, **3**, 1041–1044.
97 H. Pan, X. Lu, X. Yu, Y.-S. Hu, H. Li, X.-Q. Yang and L. Chen, *Adv. Energy Mater.*, 2013, DOI: 10.1002/aenm.201300139.
98 A. Rudola, K. Saravanan, C. W. Mason and P. Balaya, *J. Mater. Chem. A*, 2013, **1**, 2653.
99 H. Xiong, M. D. Slater, M. Balasubramanian, C. S. Johnson and T. Rajh, *J. Phys. Chem. Lett.*, 2011, **2**, 2560–2565.
100 S. H. Woo, Y. Park, W. Y. Choi, N.-S. Choi, S. Nam, B. Park and K. T. Lee, *J. Electrochem. Soc.*, 2012, **159**, A2016–A2023.
101 L. Zhao, H.-L. Pan, Y.-S. Hu, H. Li and L.-Q. Chen, *Chin. Phys. B*, 2012, **21**, 028201.
102 P. Senguttuvan, G. Rousse, M. E. Arroyo y de Dompablo, H. Vezin, J. M. Tarascon and M. R. Palacín, *J. Am. Chem. Soc.*, 2013, **135**, 3897–3903.
103 (*a*) Y. Park, D. S. Shin, S. H. Woo, N. S. Choi, K. H. Shin, S. M. Oh, K. T. Lee and S. Y. Hong, *Adv. Mater.*, 2012, **24**, 3562–3567; (*b*) L. Zhao, J. M. Zhao, Y.-S. Hu, H. Li, Z. B. Zhou, M. Armand and L. Q. Chen, *Adv. Energy Mater.*, 2012, **2**, 962–965.
104 A. Abouimrane, W. Weng, H. Eltayeb, Y. Cui, J. Niklas, O. Poluektov and K. Amine, *Energy Environ. Sci.*, 2012, **5**, 9632–9638.
105 V. L. Chevrier and G. Ceder, *J. Electrochem. Soc.*, 2011, **158**, A1011–A1014.
106 S. Komaba, Y. Matsuura, T. Ishikawa, N. Yabuuchi, W. Murata and S. Kuze, *Electrochem. Commun.*, 2012, **21**, 65–68.
107 S. Komaba, T. Ishikawa, N. Yabuuchi, W. Murata, A. Ito and Y. Ohsawa, *ACS Appl. Mater. Interfaces*, 2011, **3**, 4165–4168.
108 J. W. Wang, X. H. Liu, S. X. Mao and J. Y. Huang, *Nano Lett.*, 2012, **12**, 5897–5902.
109 L. D. Ellis, T. D. Hatchard and M. N. Obrovac, *J. Electrochem. Soc.*, 2012, **159**, A1801–A1805.
110 G. Deublein, H.-C. Tsai, L. Z. Zhou and R. A. Huggins, *Solid State Ionics*, 1990, **42**, 109–115.
111 T. Yamamoto, T. Nohira, R. Hagiwara, A. Fukunaga, S. Sakai, K. Nitta and S. Inazawa, *J. Power Sources*, 2012, **217**, 479–484.
112 Y. Xu, Y. Zhu, Y. Liu and C. Wang, *Adv. Energy Mater.*, 2013, **3**, 128–133.
113 J. Qian, Y. Chen, L. Wu, Y. Cao, X. Ai and H. Yang, *Chem. Commun.*, 2012, **48**, 7070–7072.
114 A. Darwiche, C. Marino, M. T. Sougrati, B. Fraisse, L. Stievano and L. Monconduit, *J. Am. Chem. Soc.*, 2012, **134**, 20805–20811.

115 L. Xiao, Y. Cao, J. Xiao, W. Wang, L. Kovarik, Z. Nie and J. Liu, *Chem. Commun.*, 2012, **48**, 3321–3323.
116 D. Su, H.-J. Ahn and G. Wang, *Chem. Commun.*, 2013, **49**, 3131–3133.
117 Q. Sun, Q.-Q. Ren, H. Li and Z.-E. Fu, *Electrochem. Commun.*, 2011, **13**, 1462–1464.
118 S. Hariharan, K. Saravanan, V. Ramar and P. Balaya, *Phys. Chem. Chem. Phys.*, 2013, **15**, 2945–2953.
119 M. C. López, P. Lavela, G. F. Ortiz and J. L. Tirado, *Electrochem. Commun.*, 2013, **27**, 152–155.
120 J. Qian, X. Wu, Y. Cao, X. Ai and H. Yang, *Angew. Chem., Int. Ed.*, 2013, **52**, 4633–4636.
121 Y. Kim, Y. Park, A. Choi, N.-S. Choi, J. Kim, J. Lee, J. H. Ryu, S. M. Oh and K. T. Lee, *Adv. Mater.*, 2013, **25**, 3045–3049.
122 Z. Chen, J.-Y. Choi, H. Wang, H. Li and Z. Chen, *J. Power Sources*, 2011, **196**(7), 3673–3677.
123 J.-S. Lee, T. Lee, H.-K. Song, J. Cho and B.-S. Kim, *Energy Environ. Sci.*, 2011, **4**(10), 4148–4154.
124 A. D. Martin and J. H. Zhu, *ECS Electrochem. Lett.*, 2012, **1**(1), A13–A16.
125 K. M. Abraham and Z. Jiang, *J. Electrochem. Soc.*, 1996, **143**, 1–5.
126 P. G. Bruce, S. A. Freunberger, L. J. Hardwick and J.-M. Tarascon, *Nat. Mater.*, 2012, **11**, 19–29.
127 S. A. Freunberger, Y. Chen, Z. Peng, J. M. Griffin, L. J. Hardwick, F. Bardé, P. Novák and P. G. Bruce, *J. Am. Chem. Soc.*, 2011, **133**, 8040–8047.
128 B. D. McCloskey, D. S. Bethune, R. M. Shelby, G. Girishkumar and A. C. Luntz, *J. Phys. Chem. Lett.*, 2011, **2**, 1161–1166.
129 P. Hartmann, C. L. Bender, M. Vračar, A. K. Dürr, A. Garsuch, J. Janek and P. Adelhelm, *Nat. Mater.*, 2013, **12**, 228–232.
130 S. K. Das, S. Xu and L. A. Archer, *Electrochem. Commun.*, 2013, **27**, 59–62.
131 E. Peled, D. Golodnitsky, H. Mazor, M. Goor and S. Avshalomov, *J. Power Sources*, 2011, **196**, 6835–6840.
132 E. Peled, D. Golodnitsky, R. Hadar, H. Mazor, M. Goor and L. Burstein, *J. Power Sources*, DOI: 10.1016/j.jpowsour.2013.01.177, in press.
133 Q. Sun, Y. Yang and Z.-W. Fu, *Electrochem. Commun.*, 2012, **16**, 22–25.
134 W. Liu, Q. Sun, Y. Yang, J.-Y. Xie and Z.-W. Fu, *Chem. Commun.*, 2013, **49**, 1951–1953.